AES/TG/12-09 **Leak-off of oil-based drilling fluids in saturated porous media: a CT scan-aided study**

June 2012 **Dorien Marieke Frequin**

Department of Geotechnology

Delft University of Technology

Title	:	Leak-off of oil-based drilling fluids in saturated porous media: a CT scan-aided study
Author	:	Dorien Marieke Frequin
Date	:	28 June 2012
Professor	:	P.L.J. Zitha
Supervisor	:	P.L.J. Zitha
TA Report number	:	AES/TG/12-09

Postal Address	:	Section for Petroleum Engineering
		Department of Applied Earth Sciences
		Delft University of Technology
		P.O. Box 5028
		The Netherlands
Telephone	:	(31) 15 2781328 (secretary)
Telefax	:	(31) 15 2781189

Table of Content

Acknowledgements

Performing this research and writing this report I received help, guidance, tips and advice in various ways from a lot of people. First I would like to thank my supervisor, Pacelli Zitha, for giving me a lot of freedom to perform this study and for his help and availability whenever I needed it. Gerard de Blok is kindly thanked for his support and effort on a distance; it was nice to talk to someone about the field operations and to put the research in perspective.

Next I would like to thank Eric van Beest, Hans Bruining and Hua Guo that they agreed on being part of my graduation committee. The time you made to read my report and to be present at the defence is highly appreciated.

A special thanks goes out to Marc Friebel for his technical support and patience and to Ellen Meijvogel-De Koning for her thorough assistance with the CT scanner. Furthermore I would like to thank Hua Guo also for explaining the drilling fluid preparation, Arjan Thijssen for his help with the ESEM, Dick Delforterie for the preparation of the cores and Paul Vermeulen for setting up the data acquisition. Thanks also to Wim Verwaal for helping out with the necessary porosity and permeability measurements and to Siavash Kahrobaei for his support on the Matlab scripts to visualise the CT scan data.

Besides that I would like to thank the other graduating students; Chris, Nanne, Rutger, Pieter, Andrina, Evert, Louise and Joelle for the great time we had on the ‘afstudeerzolder’ and the enlightening conversations during our coffee and lunch breaks. Thanks to my friends for putting up with me especially to the end of my research and in particular Andrea for her support and good advice on a distance. Last but not least I would like to thank my parents and sisters, for always being there and believing in me no matter what.

Abstract

The static leak-off of oil-based drilling mud into liquid-saturated cores was studied experimentally. A simple model for the leak-off was first developed extending an earlier model for the static filtration into unsaturated core. CT scan aided static filtration experiments were performed in brine and oil and brine saturated cores, simulating reservoir saturation regimes. Formation of external filter cake and internal filtration of solid particles were visualized and leak-off volumes were determined as function of time. At the end of the experiments the formed external filter cake and internal particle deposition were characterised with the aid of an Electron Scanning Microscope. Using drilling fluids containing carbonate particles it was found that leak-off volumes for saturated cores are larger than for unsaturated cores. It was observed further that leak-off volumes increase with the particle size, i.e. consistently with a more permeable external filter cake and limited internal filtration. Leak-off volumes decreased when using smaller hematite particles or using larger range of (barite) particles sizes. The filtration volumes for the smaller sized drilling fluid components in brine saturated core experiments were found to be larger than filtration volumes found for dry core experiments in previous work.

1. Introduction

The petroleum industry is moving progressively from conventional to unconventional oil and gas resources. A high technological standard is needed to explore and develop in high pressure and high temperature (HPHT) fields and to drill deep water- and extended reach wells. Nowadays oil based drilling fluids are commonly used worldwide, because of their stability at HPHT conditions.

Leak-off of drilling fluids into the formation is a recurring problem during drilling operations. It leads to loss of costly drilling fluids, wellbore instability, poorer cooling of the drill bit, formation damage, loss of rheology and lack of cuttings transportation to the surface. These factors reduce drastically the technical efficiency and the safety of drilling operations (Bourgoyne et al., 1991). Despite the higher costs and more intense pollution control procedures, oil-based drilling fluids are upcoming in use at the expense of water-based drilling fluids. This is caused by the non-corrosive character of the oil-based fluid and the beneficial rheological characteristics at high temperature.

Fluid leak-off leads to losses of drilling fluid, called matrix losses, which can be quite expensive. Lost circulation leads to lowering of pressure in the annulus inviting the possibility of reservoir fluid influx, especially in high pressured formations. This can lead to a 'kick' endangering the safety of the drilling crew and the drilling operation. Filter cake formation, both external and internal, during drilling operations leads to narrowing of the borehole down hole and internal formation damage in the drilled formation respectively. The first can cause problems continuing the drilling operation and the latter becomes a large disadvantage in reservoir zones when getting the well on to production.

Better understanding of leak-off mechanisms will help reducing drilling downtime (Tare et al., 2001), minimise fluid losses (Rojas et al., 1998) and internal filter cake formation (Bailey et al., 2000) and increase knowledge of down hole conditions (Walker and Black, 1993). Besides reduced drilling costs (Romero et al., 2006), the safety and success of drilling operations will increase. For these reasons much effort was devoted to gain better understanding of the leak-off process.

Leak-off into permeable formations leads to deposition of an external filter cake on the formation surface and an internal filter cake within the formation (Pang and Sharma, 1997). Fast initiation of the external filter cake minimizes or may even prevent fluid leak-off. This is especially true for oil-based fluids as they tend to produce filter cakes having lower permeability than water-based fluids (Aston et al., 2002; Cobianco et al., 2001; Herzhaft et al., 2001). Studies have been conducted to understand the filtration mechanisms governing fluid leak-off and several models have been introduced on external filter cake build-up and deep bed filtration (Civan, 1994; Herzig et al., 1970; Liu and Civan, 1996; Nunes et al., 2010; Pang and Sharma, 1997; Saraf et al., 2010). Several elementary mechanisms are responsible for the deposition of particles in a porous medium depending on both the characteristics of the particles and the medium (Herzig et al., 1970). They and (Sharma and Yortsos, 1987) also introduce two parameters for the internal filtration, the filtration coefficient and formation damage coefficient, used to characterise deep-bed filtration (Bedrikovetsky et al., 2001; Bedrikovetsky et al., 2003). Although extensive research has been performed a general application for field situations does not exist.

This work is based on the static filtration model developed earlier (Hua et al., 2010) and is a detailed extension of the study of the static filtration process in dry sandstone cores reported by (van Overveldt, 2011). In this study amongst others barite and gilsonite were used as an additive in the base drilling fluid. The focus of this work is on oil-based mud and on saturated sandstone cores to enable comparison with the

field conditions. Experiments were carried out using a new proposed experimental approach (van Overveldt, 2011), improving previously used standard HTHP press test with API filter paper (Aston et al., 2002; Hua et al., 2010) by conducting core flow tests through sandstone cores. The use of CT scans to visualise and quantify the leak-off of drilling fluid has been proven before (Al-Abduwani et al., 2005; Saraf et al., 2010). The microstructure of the external and internal filter cake resulting from the infiltration are examined by Scanning Electron Microscopy (SEM) and Energy-Dispersive X-ray Spectroscopy (EDS) (Byrne et al., 2000).

The objective of this study was to investigate the leak-off process of a calcium carbonate drilling fluid into 1) dry cores, 2) oil saturated cores at connate water saturation and 3) fully brine saturated cores. To produce a low permeability external filter cake an experiment was performed with smaller sized hematite particles in the drilling fluid. To place the experiments in the right context an extensive literature review was performed. This was followed by the development of a model complementing the experiments. The experiments conducted were (saturated) core flow tests with the set-up positioned in a CT scanner to visualise and quantify the leak-off process. The microstructure of the external and internal filter cake were examined by Scanning Electron Microscopy (SEM) and Energy-Dispersive X-ray Spectroscopy (EDS).

2. Leak-off during drilling operations

This chapter aims to place this research in the perspective of actual drilling operations. First general properties of oil-based drilling fluids are discussed, focusing on leak-off characteristics. Then an overview of the drilling circulation system is presented followed by a description of common practises during circulation losses. To conclude the relation between laboratory experiments and leak-off in the field is discussed.

2.1 Oil-Based Drilling Fluids

The composition of the oil-based drilling fluid used in this study is given in Table 1. It is prototypical of oil-based drilling fluids used in drilling operations. The emulsifier enables water droplets to be dispersed in the oil phase. Solid particles control the drilling fluid for viscosity, density, filtration and alkalinity. Common additives for viscosity control are asphalts and bentonite. The latter is used in the drilling fluids in this study. The density of the oil based drilling fluid is commonly controlled by barite or calcium carbonate. Lime is used to control the alkalinity, corrosion control and to optimize emulsifier performance (Bourgoyne et al., 1991). The wettability agent makes solids which are originally water-wet become oil-wet ensuring the solids suspend in the oil phase. When drilling into the reservoir formation calcium carbonate is preferred above barite because of the relative easy removal by use of an acid flush (Al-Riyamy and Sharma, 2004). A variety of additives is used for filtration control: asphalt, polymers (Lord et al., 1998), manganese oxide, xanthan gum (Cobianco et al., 2001; Navarrete et al., 2000), lignite (Kelessidis et al., 2007) and gilsonite.

Oil-based drilling fluids are complex fluids and, in general, their flow behaviour cannot be described by the Newtonian model. The flow behaviour of oil-based drilling fluids is better described using one of the following non-Newtonian models: Power-Law, Bingham Plastic and Herschel-Bulkley. The derivations for these models applied to the drilling process can be found elsewhere (Bourgoyne et al., 1991; van Overveldt, 2011).

2.2 Drilling Circulation System

Figure 1 shows a schematic overview of the drilling circulation system on a typical drilling rig. The drilling fluid is pumped down the drill string, injected through the nozzles in the bit and flows up the annulus back to

the surface. After separation of the cuttings the drilling fluid is treated and prepared to flow back down again. The main parameters controlling drilling fluid circulation are the flow rate and the pump pressure. When loss of circulation is not expected, it is not common practise to measure the amount of drilling fluid flushing back to the surface. When loss of circulation is expected, from earlier experience of drilling in the same area or detailed knowledge of the geology of the target formations the circulation is monitored. Either the flow back up the annulus is measured by a return flow meter, e.g. a Coriolis flow meter (Saasen et al., 2009), the volume in the active mud tanks is monitored for gains and losses or a differential flow meter detects the differences in pump line and return line (de Blok, 2012).

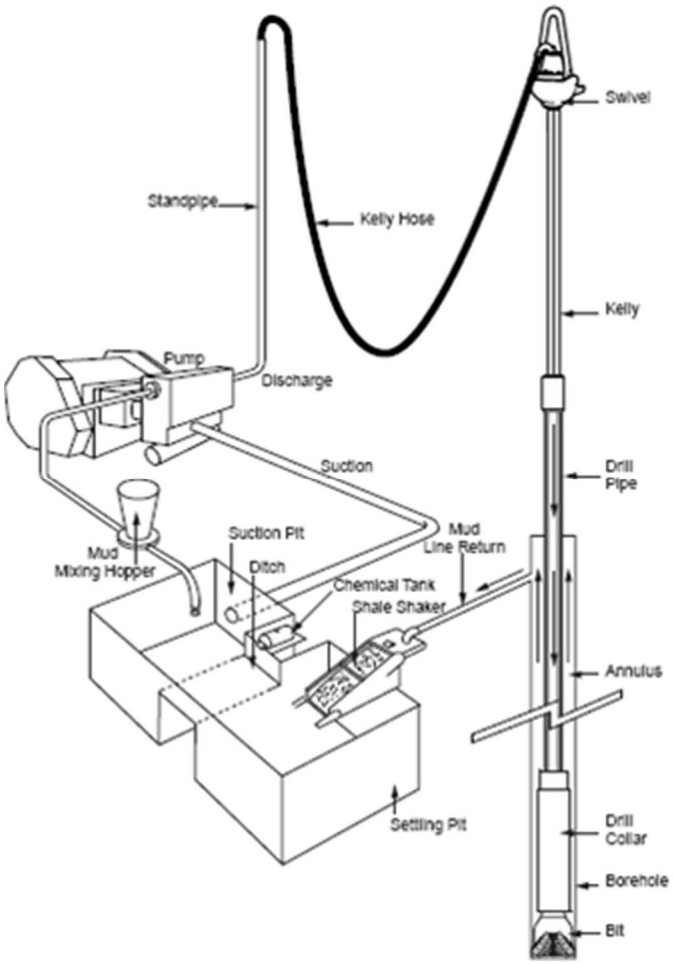

Figure 1: Mud circulation system during drilling operations

2.3 Common Practises during Circulation Losses

A division is made between lost circulation, the loss of the whole drilling mud, and down hole fluid losses associated with the leak-off and filtration process. The course of action taken when fluid losses are detected depends on several parameters: severity of the losses, expected impact on drilling time and costs, availability of a leak-off control agent. To evaluate the severity of the losses and determine the plan of action, the losses are classified in four main categories: 1) Seepage losses (1-10%) 2) Partial losses (11-65%) 3) Severe losses (66-99%) 4) and No returns (100% losses). Seepage losses are treated, depending on urgency to solve the

problem and costs, by increasing the concentration and size of the leak-off control material in the drilling fluid. Partial losses up to 35% are treated by pumping a pill or sweep to seal the loss zone in combination with increasing the leak-off control concentration in the drilling fluid when circulation is started again. Encountering partial losses of 36-75% a pill of high concentration Lost Circulation Material (LCM) is pumped. Various materials function as LCM to stop loss of circulation, some examples are: asphalt, sized salt, nutshells, calcium carbonate, hay, shredded paper and graphite. To stop severe losses a high concentration pill in a large volume is pumped followed by a high fluid loss squeeze. In case of no return a high fluid loss squeeze is pumped in order to seal the loss zone. The chosen solution to reduce and stop leak-off is often based on experience of the driller.

Another method of controlling fluid losses is Managed Pressure Drilling (MPD). This is an advanced form of primary well control usually with a closed and pressurizable drilling fluid system. That system allows more precise control of the wellbore pressure profiles than mud weights and mud pump adjustments alone (Hannegan and Fisher, 2005). This method is however more applicable to fracture losses as the hydrostatic pressure in the well can be managed by limiting the surface pressure.

2.4 Relation of laboratory tests and leak-off in the field

The wide diversity in field conditions makes it practically impossible to develop drilling fluids and leak-off control agents that will perform well at all field conditions. The basic drilling fluid composition can be standardized however adjustments have to be made to prepare the fluid for specific field conditions. Ideally these preparations are made in advance, but this is often not the case.

The development of drilling fluids relies largely on laboratory experiments. These tests are however not able to reproduce all field characteristics but they should represent the key features of the process that is studied. Leak-off processes are often studied using dynamic and static filtration tests (Walker and Black, 1993). The application of both modes in the drilling process is illustrated in Figure 2. Dynamic filtration experiments represent the leak-off process during circulation of the drilling mud better than static experiments. However, the tests reported in literature cannot reproduce the flow regimes and areas encountered in the field (Cobianco et al., 2001; Lord et al., 1998). Besides dynamic tests are more difficult to set-up and execute than static tests.

In this work, static filtration experiments were preferred to isolate the filtration process from the flow. This way the resulting erosion and compression of the external filter cake during dynamic conditions are not taken into account (Clark and Barkat, 1990).

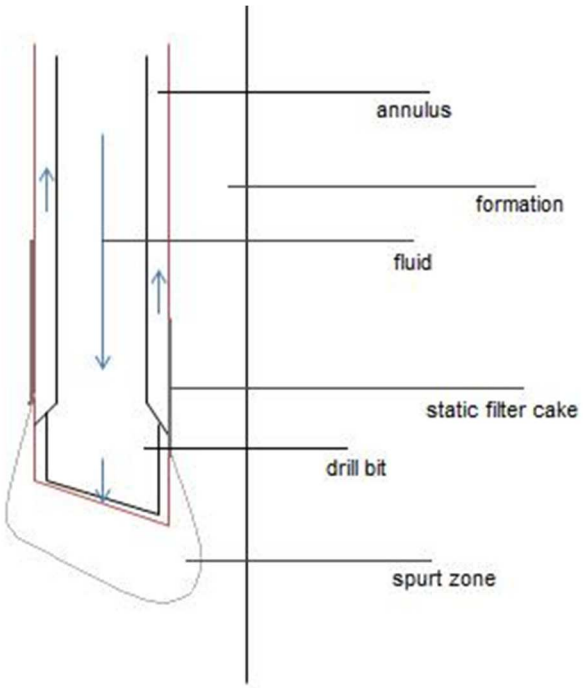

Figure 2: Cross section of a drill bit with spurt zone, illustrating both static and dynamic filtration. Schematic after (Walker and Black, 1993)

3. Theory

3.1 Linear Filtration

As mentioned above, leak-off of drilling fluids into permeable zones leads to build-up of an external filter cake, infiltration of fluids and deposition of particles into the formation. A model for the static filtration into dry cores was presented recently (van Overveldt, 2011). In this section the model will be extended to the case for saturated cores.

3.1.1 Physical model

The problem geometry is shown schematically in Figure 3. Drilling fluid containing suspended solid particles with concentration c_p overlays a porous medium with length L, porosity ϕ and permeability k. Leak-off occurs upon applying a pressure drop ΔP. An external filter cake with thickness l_c, porosity ϕ_c and permeability k_c results on the surface area of the filtration experiment, S.

Mud flowing through the growing external filter cake into the core displaces the fluids initially present in the core. In this study two cases will be considered: a) core is initially at the connate water saturation and b) initially core is fully saturated with brine. For case a) there will be single-phase flow in both external filter cake and in the core whereas in the latter case flow through the filter cake will be single phase and flow through the porous medium will be two-phase.

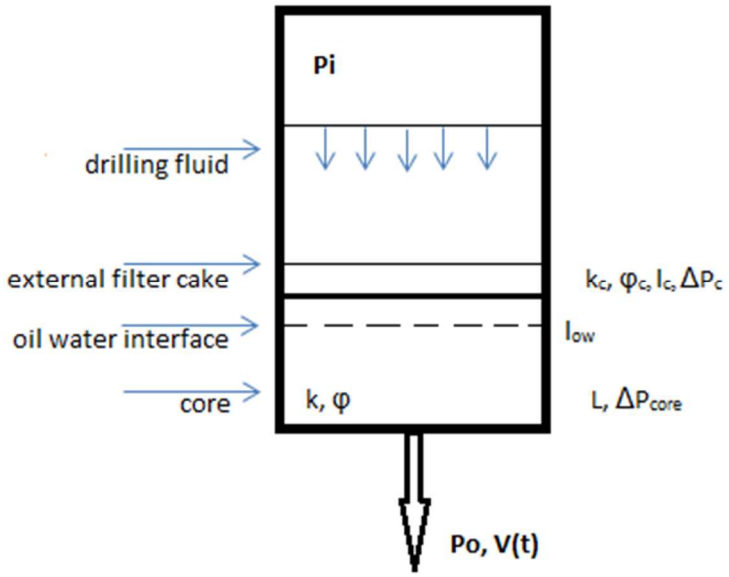

Figure 3: Schematic geometry of the model for the external filtration; the drilling fluid is pushed down, penetrating the porous medium, leaving solid particles behind which form the external filter cake. Inside the core the oil-water interface (in case of brine saturated cores) is moving downwards as time is increasing.

Expressions for the leak-off volume were derived for the two, subject to the following main assumptions: (1) solid particles and fluids are incompressible, (2) flow is laminar isothermal, (3) only the solid particles in the drilling fluid contribute to the external filter cake build-up, (4) no penetration of particles in core before experiment starts, (5) build-up of external filter cake will occur after a short spurt loss time, (6) single-phase flow through formed filter cake and single or two-phase flow through the porous medium (core).

The extended model for both cases is described below, details of the derivations can be found in Appendix I.

The thickness of the filter-cake l_c is obtained by stating that, by mass conservation, the amount of particles filtered out of the fluid equals the amount of particles deposited in the filter cake at any time t. The flow through the porous cake and the porous medium obey the classical single and multiphase flow based on mass balance and Darcy's laws.

a) Core at the connate water saturation

As already mentioned, in this case, we are dealing with single-phase flow of the drilling fluid without particles with viscosity η_o through the filter cake and through the core. The core is characterized by a relative permeability $k_{ro}(S_{wc})$ at the connate water saturation S_{wc}.

The filtration behavior can be described by:

$$Q_1 = [F_2 V(t) + 1]\frac{dV(t)}{dt} \tag{1}$$

With the constants

$$Q_1 = \frac{k}{\eta_o} S \frac{\Delta P}{L}; \qquad F_2 = \frac{c_p k k_{ro}(S_{wc})}{k_c S\big(1 - c_p\big)(1 - \phi_c) L}$$

Integrating the expression for Q_1 with $V(t_s) = V_s$ as initial condition gives for V(t):

$$V(t) = \begin{cases} Q_1 t & t < t_s \\ \dfrac{\sqrt{(F_2 V_s + 1)^2 + 2F_2 Q_1 (t - t_s)} - 1}{F_2} & t > t_s \end{cases} \tag{2}$$

Here V_s is the spurt loss volume of filtrate and t_s is the spurt loss time. When V_s and t_s equal zero, the equation for $t > t_s$ becomes:

$$V(t) = \frac{\sqrt{1 + 2F_2 Q_1 t} - 1}{F_2} \tag{3}$$

When $2F_2Q_1 >> 1$ the above equation can be approximated by:

$$V(t) = \sqrt{\frac{2Q_1 t}{F_2}} \tag{4}$$

Equation 4 shows that for an oil-saturated core the filtrate volume is proportional to the square root of time after the spurt loss time.

b) Brine saturated core: piston-like displacement

In this case oil (viscosity η_o) displaces water with viscosity η_w in piston like manner. The initial condition in the core is $S_w^0 = S_w(z, 0) = 1$.

Denoting the time dependent position l_{ow} of the oil/water front the core is at connate water saturation for $0 \le z \le l_{ow}$. The filtration behaviour can be described by (see detailed derivation in Appendix I):

$$Q_0 = [F_1 V(t) + 1]\frac{dV(t)}{dt} \tag{5}$$

Where

$$Q_0 = \frac{k}{\eta_w} S \frac{\Delta P}{L}; \qquad F_1 = \left[\frac{\eta_o}{\eta_w k_{ro}(S_{wc})} - 1\right]\frac{1}{\phi(1 - S_{wc})SL} + \frac{\eta_o c k}{\eta_w k_c S\left(1 - c_p\right)(1 - \phi_c)L}$$

With Q_0 representing the flow [volume per time] in the saturated core. Integrating with the initial condition $V(t_s) = V_s$ we obtain for $V(t)$:

$$V(t) = \begin{cases} Q_0 t & t < t_s \\ \dfrac{\sqrt{(F_1 V_s + 1)^2 + 2F_1 Q_0 (t - t_s)} - 1}{F_1} & t > t_s \end{cases} \tag{6}$$

When V_s and t_s equal zero, the equation for $t > t_s$ becomes:

$$V(t) = \frac{\sqrt{1 + 2F_1 Q_0 t} - 1}{F_1} \tag{7}$$

When $2F_1Q_0 >> 1$, Equation 7 can be approximated as

$$V(t) = \sqrt{\frac{2Q_0 t}{F_1}} \tag{8}$$

Equation 8 shows the square root of time dependency of the filtrate volume after the spurt time.

c) Brine saturated core: Buckley Leverett displacement

Now we consider the case where idealised piston-like water displacement by oil does not occur. This is done replacing the assumption of idealised piston-like flow behaviour for the two-phase flow in the porous medium by the Buckley-Leverett equation. Other assumptions and the initial conditions are as above. The leak-off volume obeys the following equation:

$$Q_0 = [F_4 V(t) + 1]\frac{dV(t)}{dt} \tag{9}$$

This equation is similar to Equation 5 but in the present case the constant F_4 is given:

$$Q_0 = \frac{k}{\eta_w} S \frac{\Delta P}{L}; \qquad F_4 = \left[\frac{\eta_o \bar{f}_o(w)}{\eta_w k_{ro}(S_{wc})} - 1\right]\frac{1}{\phi(1 - \bar{S}_{w(t)})SL} + \frac{\eta_o c k}{\eta_w k_c S(1 - c_p)(1 - \phi_c)L}$$

This function assumes that F_4 is constant which is a reasonable approximation. $\bar{S}_{w(t)}$ is the average water saturation as a function of time and $\bar{f}_o(w)$ is the average fractional flow of oil in the brine saturated core. Now the filtrate volume as a function of time is

$$V(t) = \begin{cases} Q_0 t & t < t_s \\ \dfrac{\sqrt{(F_4 V_s + 1)^2 + 2F_4 Q_0 (t - t_s)} - 1}{F_4} & t > t_s \end{cases} \tag{10}$$

When V_s and t_s equal zero, the equation for $t > t_s$ becomes:

$$V(t) = \frac{\sqrt{1 + 2F_4 Q_0 t} - 1}{F_4} \tag{11}$$

When $2F_4Q_0 >> 1$ equation 11 can be approximated as

$$V(t) = \sqrt{\frac{2Q_0 t}{F_4}} \tag{12}$$

Equation 12 shows the square root of time dependency of the filtrate volume after the spurt time.

4. Experiments

4.1 Materials and methods

Brine used to saturate the core was 3.5 wt% NaCl solution, a composition comparable to the composition of Sea water. The base oil is Sipdrill 2/0. The composition of the oil based mud is shown in Table 1. To prepare the mud, first the required amount of Sipdrill 2/0 base oil was measured and mixed with the primary emulsifier (OmniMul, manufactured by Baker Hughes) using an IKA mixer for 3 minutes while increasing rotation speed gradually up to 5000 rpm. At the same time the water phase was prepared by adding the appropriate amount of $Ca(OH)_2$ to the water and this was mixed with a magnetic stirrer until all the salt was dissolved. The water phase was then added to the oil phase to prepare the emulsion, mixing continued for 5 minutes. Next bentonite and secondary emulsifier OmniChem from Baker Hughes were added while mixing for another 5 minutes. Finally calcium carbonate was added and mixing continued for an additional 15-20 minutes at 5000 rpm. Because OmniChem is not manufactured anymore, a new wettability control agent Dril Treat from Halliburton was used for one experiment. This was done to compare the influence of OmniChem and Dril Treat on the leak-off process. The corresponding results are presented in Appendix III.

Table 1: Drilling fluid components and characteristics

Component	Specific Gravity	Weight%
Base oil	0.81	36
Water	1.00	12
OmniMul (emulsifier)	0.95	3
OmniChem (wettability control)	1.00	1
Lime [$Ca(OH)_2$]	2.24	2
Bentonite (viscosity control)	2.40	2
Calcium carbonate	2.71	44
Barite (density control)	4.20	57.2
Hematite	5.30	59

4.2 Experimental set-up

The experimental set-up is shown schematically in Figure 4. It consists of a core holder which is described in more details below, a pump to inject the brine and oil and a pressure gauge monitoring the pressure above the core. A differential pressure gauge was used to measure the pressure drop during saturation, a CO_2 vessel to supply the CO_2 flush and a back pressure for the flush and brine saturation. A balance was used to monitor the effluent and the data was recorded by the data acquisition system.

4.3 Core and core holder

The properties and dimensions of the sandstone core are listed in Table 2. The core-holder is shown schematically in Figure 4. It consists of a PEEK-cylinder, bottom and cover, which are transparent to X-rays. The sandstone core is placed at the bottom of this cylinder. A cylinder (transparent to X-rays) is placed in the upper part of the core holder, which will contain the brine, oil and the drilling fluid. At the top of the core-

holder a tube is the inlet for the drilling mud, a second tube is used to pressurize the system with air. The tube at the bottom of the core holder is used to inject the brine and to discharge the effluents.

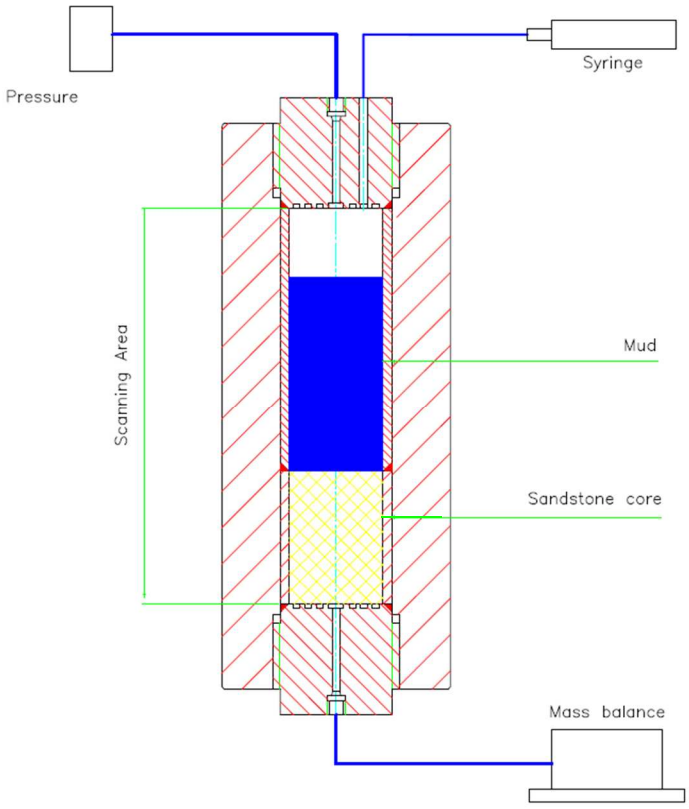

Figure 4: Schematic of the core holder, injection tubes and outlet tube

Table 2: Properties and dimensions of the core

Material	**Bentheim Sandstone**
Porosity [%]	24 ± 1
Permeability [D]	2.3 ± 0.2
Length [cm]	5.8 ± 0.1
Diameter [cm]	3.8 ± 0.1
Pore Volume [cm^3]	13 ± 0.5
Pore Size Average [µm]	17 ± 5

4.4 CT scanning

The core holder is vertically positioned in a third generation SAMATOM Plus4 Volume Zoom Quad Slice Scanner to obtain the CT scans. A picture of the experimental set-up inside and around the CT scanner is presented in Figure 5. The main concept of a CT scanner is sending out a beam of x-rays from different angles through the object of interest. The device measures the linear attenuation (μ [m^{-1}]) which describes the fraction of the x-rays that is scattered per unit thickness of the object of interest (Vinegar and Wellington 1986) and creates a cross-sectional image of attenuation coefficients. In practise the attenuation is expressed in Hounsfield Units (HU). A more detailed explanation of the attenuation coefficient, the Hounsfield Unit and the CT scanner is presented in Appendix II. CT scans were made parallel to the main core axis. The imaging settings of the CT scanner are listed in Table 3. At the beginning of an experiment the CT scans were shot at a short time intervals of 6, 10 and 30 seconds where after the time intervals were increased to 1, 5 and 10 minutes. This method proved accurate for visualizing and quantifying the leak-off process (van Overveldt, 2011).

Table 3: Image settings CT scanner

Description	Conditions
Voltage	140 kV
Current	250 mA
Slice Thickness	1 mm and 2.5 mm
Voxel Size	0.3 mm
Scan Mode	Sequential

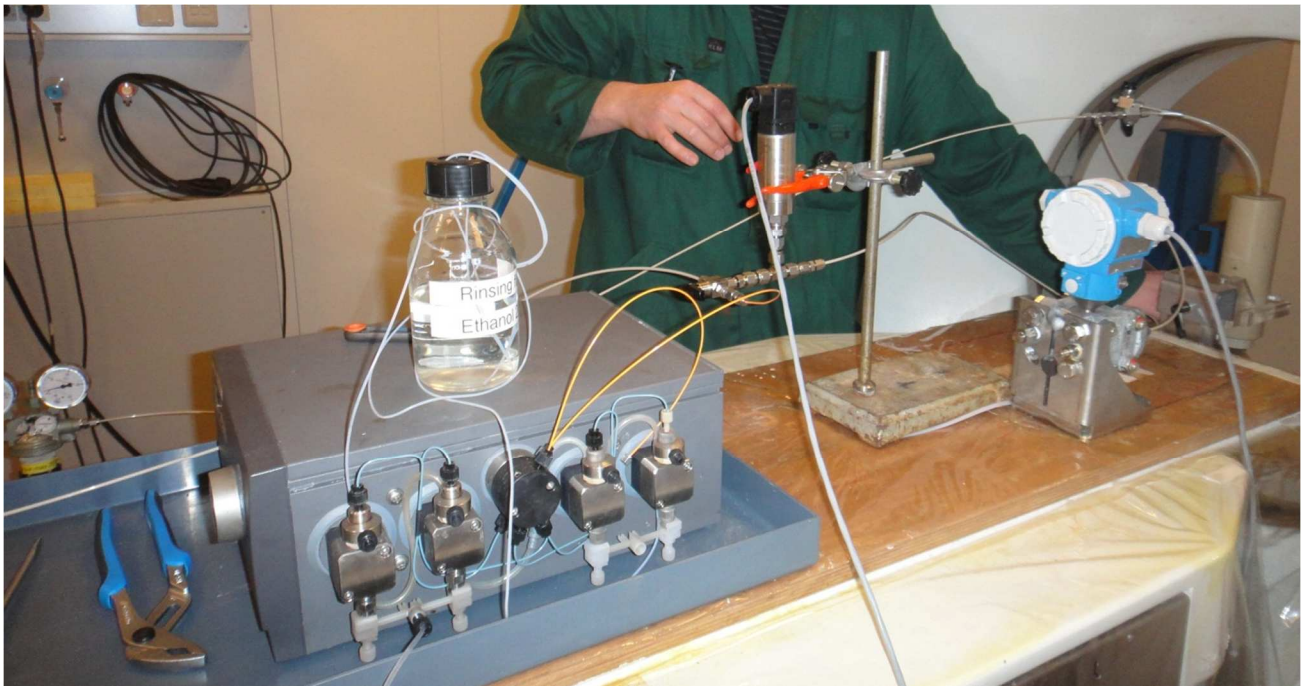

Figure 5: Picture of the experimental set-up. From left to right: CO_2 supply, pump used for saturation with brine and oil, pressure gauge, pressure differential gauge, core holder and CT scanner. Not on the picture are the back pressure and the data acquisition system.

4.5 Experimental Procedure

4.5.1 Preparation and leak-off experiment

Each leak-off experiment was preceded by a preparation into the desired saturation state, namely full water saturated ($S_w = 1$) or connate water saturation ($S_w = S_{wc}$). The core-holder with the dry core was positioned in the CT scanner, then a scan was made to obtain the dry-core reference data. First the core was flushed from the bottom with CO_2 for about 20 minutes, at back pressure of 25 bars. The core was saturated by injecting brine from the bottom at a rate of 5 ml/min and also at back pressure of 25 bars. CT scans were made every 5 minutes to follow the saturation process. The overflow of brine was sucked out of the set-up, where after the base oil was injected into the core from the top at a rate of 5 ml/min. This drainage process was also recorded with CT scans. The overflow of oil was pushed through the core with air until only a thin (mm) layer was left on top of the core. Care was taken that there was still a thin layer of oil left on top of the core, to be entirely sure that no air had penetrated the core. Then the bottom valve was closed to prevent early penetration of drilling mud into the core when preparing the experiment.

The oil-based drilling mud was injected from the top of the core holder via a syringe through a tube, while the air supply valve (at the top of the set-up) was open to let the air in the core holder escape. The injection of drilling mud took about one minute. A CT scan was made where after the air supply was opened to pressurise the system with 8 bars, simultaneously the outlet valve was opened. Then CT scans were made at time intervals to monitor and to visualize the leak-off process. All experiments were done at ambient temperature. An overview of the experiment procedure is presented in Table 4.

Table 4: Overview of experiment procedure

Step	Procedure	Data	Remarks	Experiment nr
1	Place core holder in CT scanner	Dry core reference CT scan	Check O-rings	1 to 5
2	Flush core from bottom with CO_2 for 20 min	Pressure & differential P	BP = 25 bar	1 to 5
3	Brine injection from bottom at 5 ml/min	CT scans, Pressure & dP	BP = 25 bar	1 to 5
4	Suction of brine out of core-holder	-	-	1 to 5
5	Oil injection from top at 5 ml/min	CT scans	-	2
6	Push oil through core with air	CT scans	Leave thin oil layer	2
7	Close bottom valve	-	-	1 to 5
8	Inject drilling mud from top via syringe	-	Leave air escape open	1 to 5
9	Make CT scan of start situation	CT scan	-	1 to 5
10	Open air supply	CT scans	P = 8 bar	1 to 5

4.5.2 Overview of performed experiments

The leak-off experiments performed in this study are listed in Table 5. The variation in the experiments were 1) the fluid fill of the sandstone core, 2) the particle size of the main drilling fluid component and 3) the alternation of OmniChem and Dril Treat as wettability control agent. The drilling fluid was for all experiments prepared following the same recipe, changing only the component (Table 5). As previously mentioned these fluids have a special character and can therefore have small alternations in their behaviour which can cause slightly different leak-off volume results. All the experiments were performed twice to show reproducibility. The leak-off volume and rate were determined per experiment and matched to the theoretical model. For every first experiment the external filter cake and internal filtration were analysed and characterised using a Philips XL30 ESEM scanning electron microscope. However this was not done for the oil saturated core experiment as the equipment cannot handle the oil. Additionally an element analysis of the external filter cake and internal filtration was performed by EDS (Energy-Dispersive X-ray Spectroscopy) using an EDAX system, type Phoenix.

Table 5: Overview of performed experiments

Exp nr	Initial Core Saturation	Component	Particle d_{50} [mm]	Remarks
1A	Dry	Calcium Carbonate	14	
1B	Dry	Calcium Carbonate	14	
1C	Dry	Calcium Carbonate	14	Dril Treat
2A	Oil ($S_w = S_{wc}$)	Calcium Carbonate	14	
2B	Oil ($S_w = S_{wc}$)	Calcium Carbonate	14	
3A	Brine ($S_w = 1.0$)	Calcium Carbonate	14	
3B	Brine ($S_w = 1.0$)	Calcium Carbonate	14	
4	Brine ($S_w = 1.0$)	Barite	-	
5A	Brine ($S_w = 1.0$)	Hematite	5	
5B	Brine ($S_w = 1.0$)	Hematite	5	

5. Results and Discussion

In this chapter the results of this study will be presented and discussed. The data analysis procedure is explained for the first experiment and is similar for the other experiments. The results of the repeat experiments can be found in Appendix III.

5.1 Dry Core Leak-off Experiment

5.1.1 CT scan images and attenuation profiles

Figure 6 shows a CT scan image for the dry core experiment (1A, see Table 5) shot after 6 seconds and Figure 7 represents the attenuation profile corresponding to that image. The CT scan image is an averaged image of four parallel images (Table 3) shot at the same time step with a spacing of 0.5 mm. In the image the dark blue represents air, the blue-green is the drilling fluid and the orange block is the core. The light blue surrounding is the core holder and the flashing red dots are the O-rings, used to seal the set-up. The small orange part at the top of the core shows the leak-off of fluid into the core. Attenuation profiles are obtained by averaging the CT scan values perpendicularly to the core length at various times.

The x-axis of the attenuation profile graph represents the position in the core holder; zero mm corresponds to the top of the image in Figure 6. The y-axis shows the attenuation coefficient in Hounsfield units (HU) measured by the CT scanner at a certain point along the core holder. The change from air to drilling fluid is indicated in Figure 7 by the left vertical line. The middle vertical line represents the change in attenuation coefficient caused by the change from drilling fluid to core. The graph shows the attenuation coefficient of the drilling fluid is around 1500 HU and of the core around 2300 HU. The vertical lines representing the air-drilling fluid interface move from left to right as a function of time (Figure 9). The leak-off volume of drilling fluid into the core is extracted from these shifts of the interface in space. The drilling fluid-core interface moves in the opposite direction (right to left), showing the build-up of the external filter cake on top of the core.

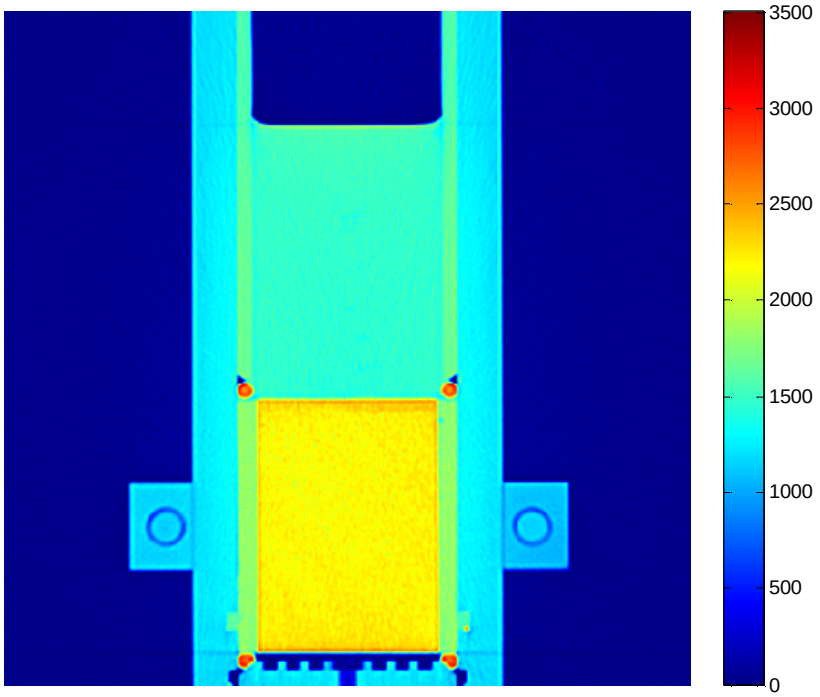

Figure 6: CT Scan image of experiment 1A, shot after 6 seconds after applying air pressure. The dark blue represents air, green is the drilling fluid and yellow the core. The light blue surrounding is the core holder and the bright red spots the sealing O-rings. The orange at the top of the core shows already some leak-off of fluid into the core.

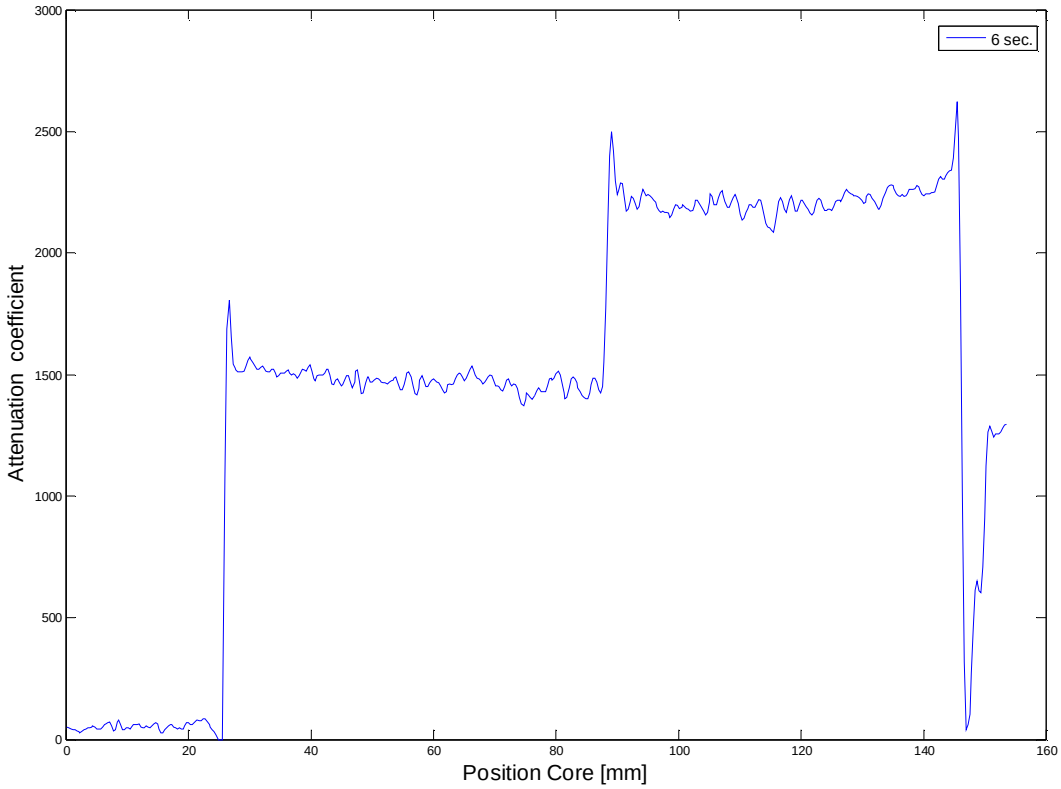

Figure 7: Attenuation profile for experiment 1A corresponding to the CT scan image shot after 6 seconds (Figure 6), with the left vertical line representing the air-drilling fluid interface and the middle vertical line representing the drilling fluid-core border

Figure 8 shows CT scan images of experiment 1A at different times, visualising the fluid leak-off into the core and the external filter cake build-up. In the start image no significant infiltration of drilling fluid or external filter cake formation is observed. The image shot after 6 seconds shows a small amount of drilling fluid infiltration into the core. After 56 seconds a small external filter cake is visible and the internal filtration is expanding into the core. At 12 minutes the external filter cake has become thicker and the fluid penetration did not break through the core yet. At 23 minutes the fluid has passed through the whole core. It was tried to visualise the fluid interface in the core with the attenuation profiles, but the difference in attenuation coefficient was not sufficient to rise above the noise level. In Figure 8 all images from left to right it is seen that the drilling fluid level drops. This drop in drilling fluid level represents the leak-off volume, penetrating the core. In total 29 images are shot throughout a time span of 1.5 hours, from which the leak-off volume as a function of time is determined (Figure 10). The experiment is repeated to show the reproducibility by comparing the leak-off volumes. The corresponding CT scan images and attenuation profiles of this repeat experiment can be found in Appendix III.

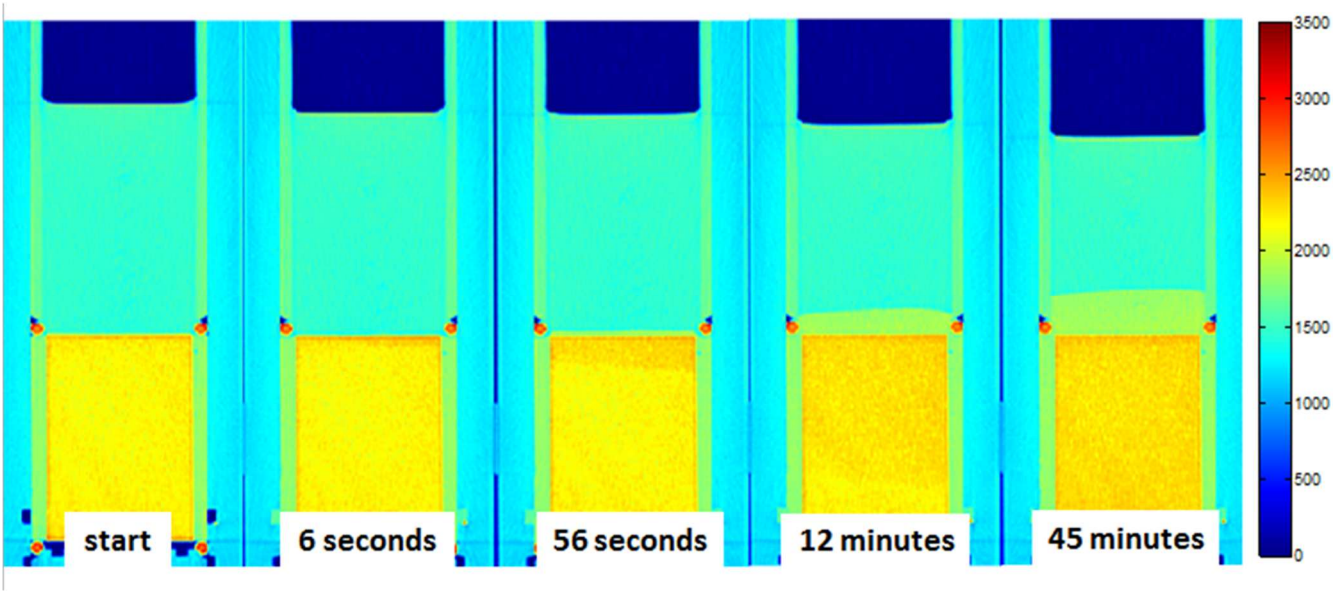

Figure 8: CT scan images of experiment 1A at different times, visualising the leak-off process and used to construct the attenuation profiles

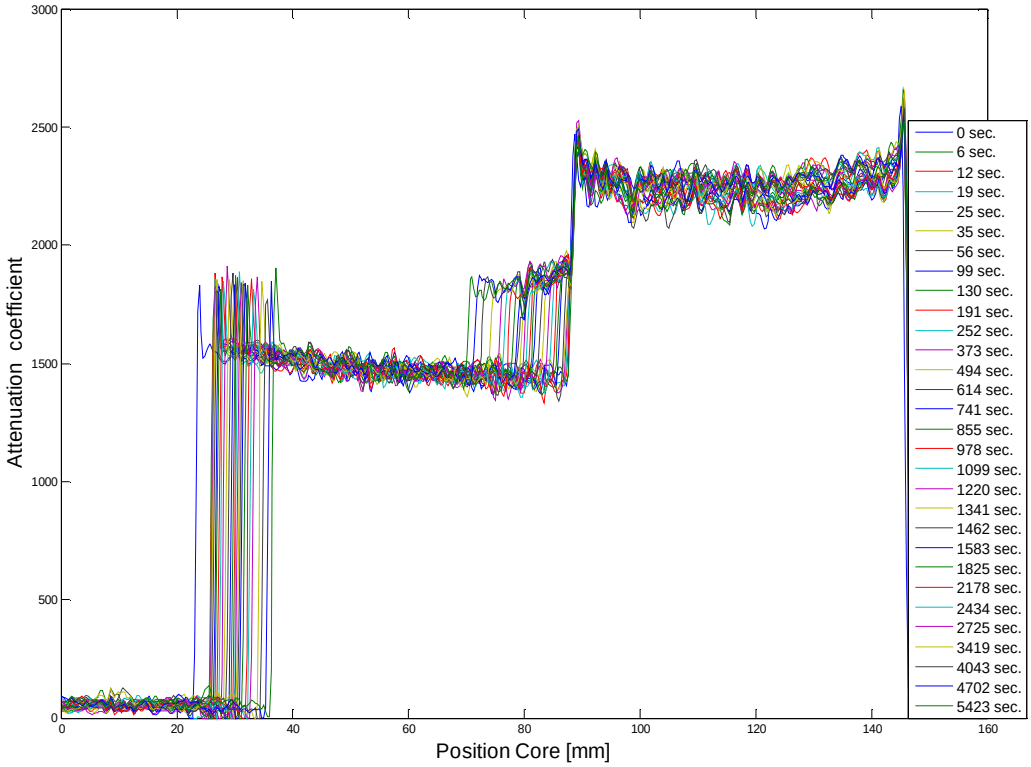

Figure 9: Attenuation profiles at different times for experiment 1A, created from CT scan images, used to determine the leak-off volume

5.1.2 Leak-off volume

Figure 10 shows the filtration volume plotted as a function of the square root of time for both dry core experiments (1A and 1B). The data from experiment 1C does not agree (Appendix III) and is therefore not plotted in the figure. The symbols represent the measured data and lines are least-square fit of equation 4. The filtration follows a linear relation with the square root of time after the spurt time, this is in agreement with the filtration model for dry cores in the work of (van Overveldt, 2011). The spurt loss volumes are 2.36 ± 0.05 and 1.29 ± 0.05 ml for experiments 1A and 1B, respectively. This volume is found by extrapolating the linear fit after the spurt loss and taking the intersection with time is zero (Bourgoyne et al., 1991). The difference in the spurt loss volumes is explained by the difference in start volume of the drilling fluid. For experiment 1A a larger start volume of drilling fluid was used, resulting in a higher spurt loss volume. After the spurt loss time the curves show a better reproducibility because the leak-off rate is stabilised. For drilling fluid containing barite in the same volume fraction as calcium carbonate in this study, spurt loss volumes of 0.87 ± 0.05 and 1.21 ± 0.05 ml were reported (van Overveldt, 2011). However this is in the same order of magnitude, it seems the calcium carbonate is less strong in controlling the leak-off into the porous medium. Considering the permeability difference of a factor 2 in the cores used for both experiments the difference in spurt loss cannot be compared without taking this difference into account. The leak-off represented by the steep gradient of both data curves in Figure 10 however does imply less leak-off control by calcium carbonate than barite. From both Figure 8 and Figure 10 one can also expect the external filter cake to have a relative high permeability as the drilling fluid penetrates the core at fairly high rate.

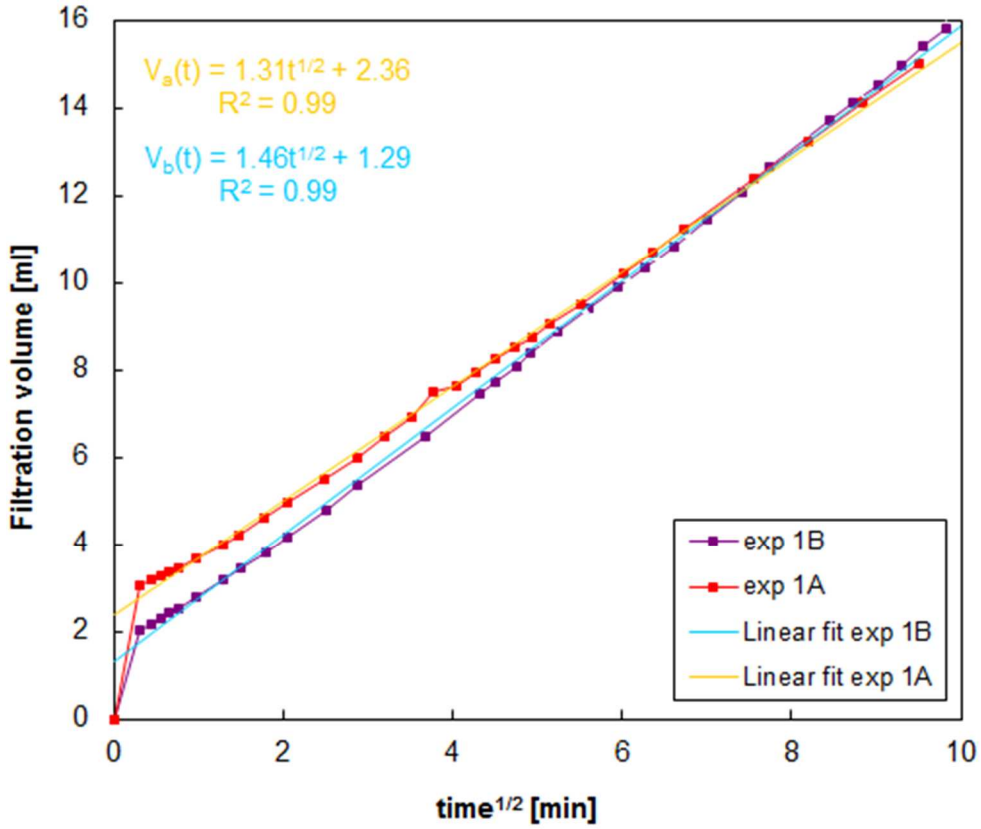

Figure 10: Filtration volume [ml] vs. the square root of time [min] for experiments 1A and 1B. The spurt loss volume is 2.36 ± 0.05 ml and 1.29 ± 0.05 ml for experiment 1A and 1B respectively.

5.1.3 External filter cake and internal filtration characterisation

The external filter cake build-up and the internal filtration are analysed and characterised with the help of a Philips XL30 ESEM scanning electron microscope. With this microscope images with a very high magnification were obtained (Figure 12). The contrast in the ESEM images is caused by the different atomic numbers of the elements present in the drilling fluid. Subsequently an elemental analysis is performed on a representative area of both the external filter cake and the internal filtration. With this analysis the difference in content is determined.

Figure 11: Top part of the core of experiment 1A, used for ESEM characterisation and external filter cake (20 ± 0.5 mm)

The top part of the core (Figure 11) is used in the ESEM characterisation (Figure 12). The external filter cake has a thickness of 20 ± 0.5 mm (Figure 11), this dimension is too large to visualise on the ESEM images. Therefore only a small part of the external filter cake was examined under the microscope. From Figure 12 it can be seen that the drilling fluid particles not only form an external filter cake but also penetrate into the core. The particles penetrating the core do not clog the pore space and transfer further into the core. This can be explained by the small size of the particles compared to the pore size. The particles do not form a dense pack, resulting in a high permeability filter cake. This is consistent with the high leak-off rate encountered. This suggests that the particle size is not the most important factor in the external filter cake build-up and the internal filtration process. The shape of the particles and different particle sizes also have influence on the way the filter cake is packed and the particles penetrated the core.

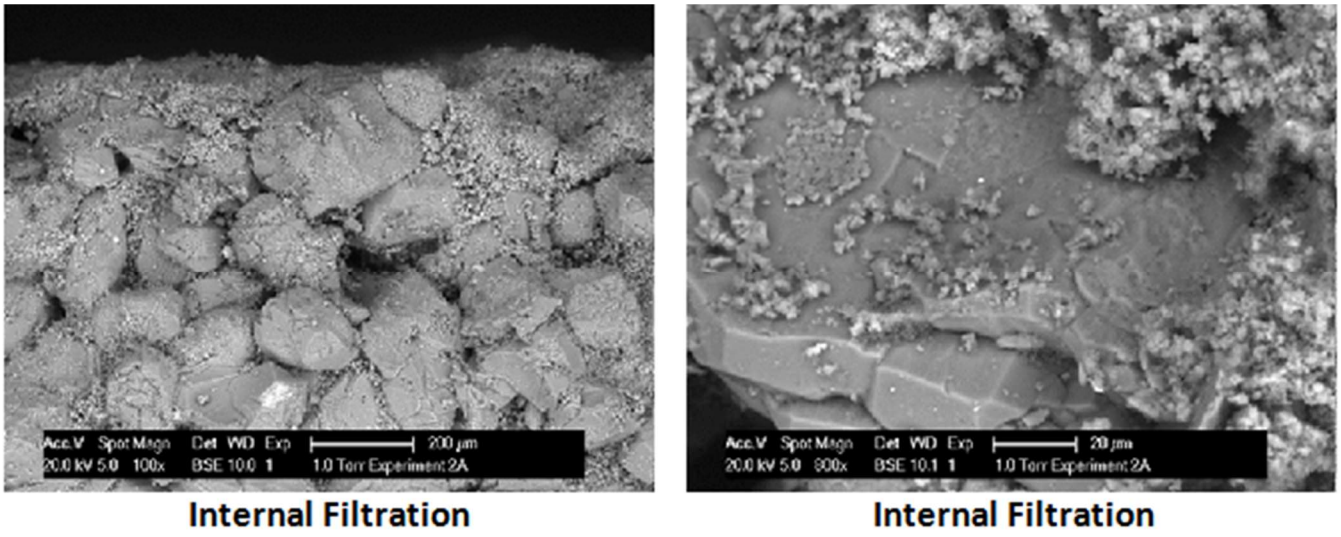

Figure 12: Images of internal filtration for experiment 1A, obtained by ESEM

An overview of the marker elements for the different drilling fluid particles is presented in Table 6. The elemental analysis in Figure 13 confirms that the external filter cake consists for the largest part out of calcium carbonate. These particles also penetrate the core. Bentonite and lime also filter into the core as well as some copper, which is present in the calcium carbonate in a very small percentage.

Table 6: Chemical formulas/components for the drilling fluid particles

Particle	Chemical formula/Components	Marker element
Bentonite	$Al_2O_34SiO_2H_2O$	Si, Al
Calcium carbonate	$CaCO_3$	Ca
Lime	$Ca(OH)_2$	Ca

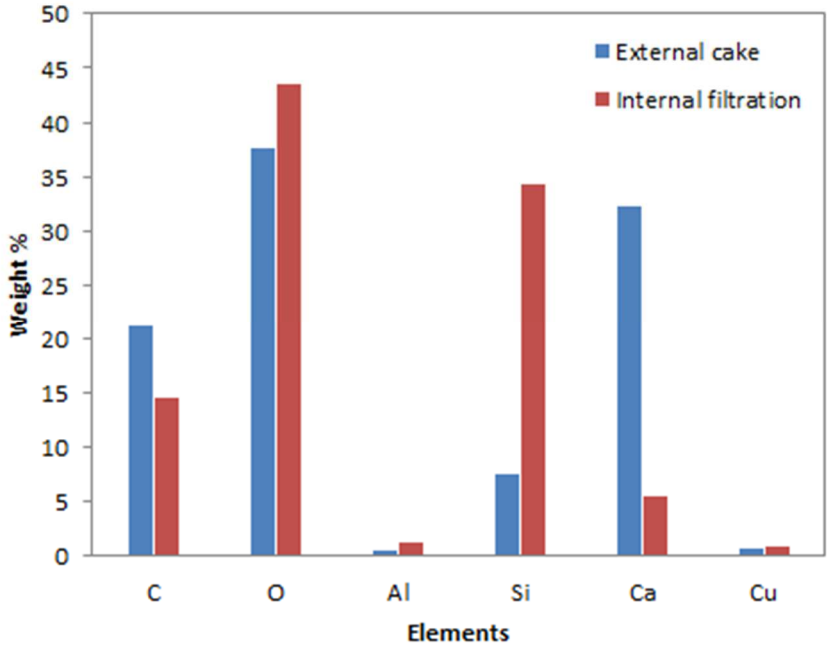

Figure 13: Elemental analysis for external cake and internal filtration of experiment 1A, obtained by EDAX. The elements are displayed in weight %. The external filter cake consists for the largest part of calcium carbonate. All particles also penetrate the core enabled by the high external filter cake permeability.

5.2 Leak-off into Oil Saturated Core

5.2.1 CT scans and attenuation profiles

Experiments 2A and 2B were performed with an oil saturated core (oil saturation equals 1-S_{wc}) and drilling fluid composition as in Table 1. Figure 14 shows CT scan images representative for the leak-off process. The start image captures the shock wave resulting from pressurizing the system. Here a very small external filter cake can be distinguished, this is in contrast with the start image of experiment 1. The images shot after 6 and 12 seconds show that the drilling fluid passes rather quickly through the formed external filter cake and the sandstone core compared to the dry core experiment. Due to the one phase flow in the core no interface as in experiment 1 is distinguished. After 18 seconds all the drilling mud has passed both the core and the external filter cake. This confirms the expected faster leak-off than for experiment 1 because of the one phase flow in the core. The very fast break through and ending of the experiment is attributed to the high permeability of both the external filter cake and the core, compared with earlier experiments (van Overveldt, 2011). The image shot after 6 minutes shows that the external filter and the core have lower attenuation coefficient (1900 and 2150 HU respectively) than previous images (for instance image at 18s). This change is also observed in the attenuation profile graph (Figure 15). This can be explained by penetration of air in the porous external filter cake and the porous medium as the fluid is completely displaced from system. The attenuation coefficient of air is lower (dark blue) than of the core; a lower value of the attenuation coefficient points out air filling the pores in the external filter cake as well as in the core.

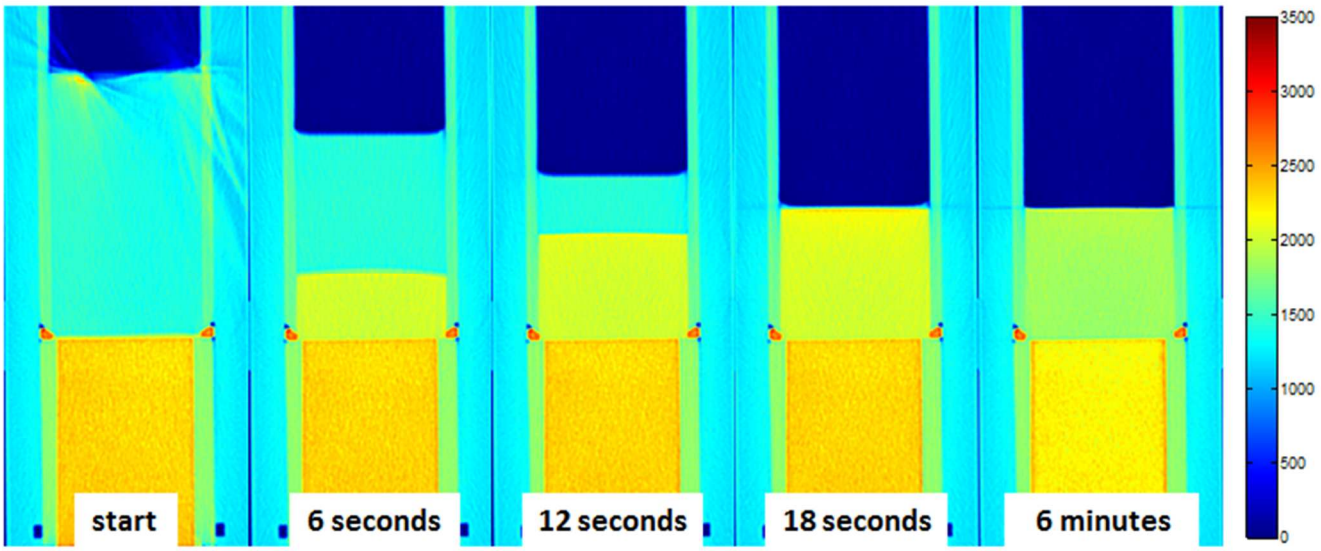

Figure 14: CT scan images of experiment 2A at different times, visualising the leak-off process and used to construct the attenuation profiles

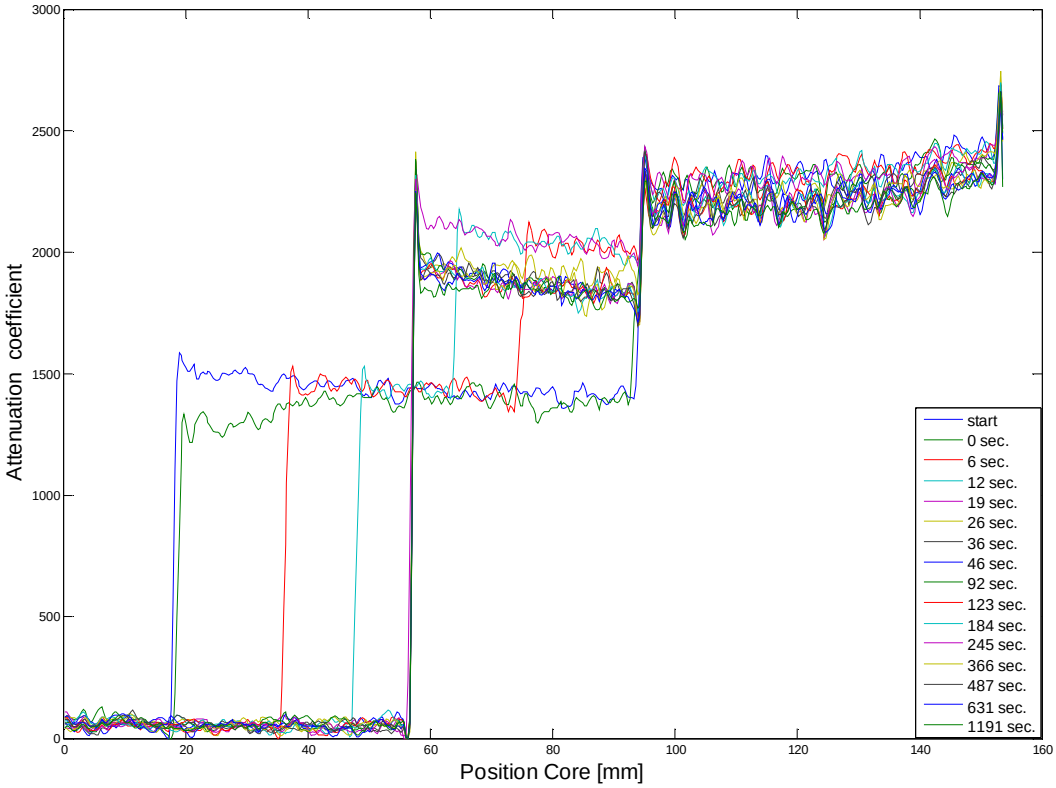

Figure 15: Attenuation profiles for experiment 2A at different times, created with CT scan images, used to determine the leak-off volume. Note the lower attenuation coefficient for the external filter cake after some time of establishment.

5.2.2 Leak-off volume

Figure 16 shows the measured (symbols) and fitted (lines) leak-off volumes as a function of the square root of time for the experiments 2A and 2B. Equation 4 was fitted to the first 3 and 2 data points obtained in experiments A and B, respectively, before complete filtration of the mud (solid lines). The found spurt loss volumes are 3.43 ± 0.05 ml and 2.32 ± 0.05 ml respectively for experiment 2A and 2B. The difference is assigned to the large difference in start volume of injected drilling fluid. The models fit the data less well than in experiment 1. This is because the values for factor F_3 and the spurt loss volume do not validate the approximation made in the theory. For experiment 2A the effluent was unsuccessfully collected by a mass fraction collector, only 18 ml of the total effluent was measured. For experiment 2B the experimental procedure was changed; the effluent was collected in a bottle on a balance. The total effluent recovered was 57 ± 0.5 ml. This is more than leak-off volume and pore volume together which can be explained by the presence of solids in the effluent, filling a part of the measured volume.

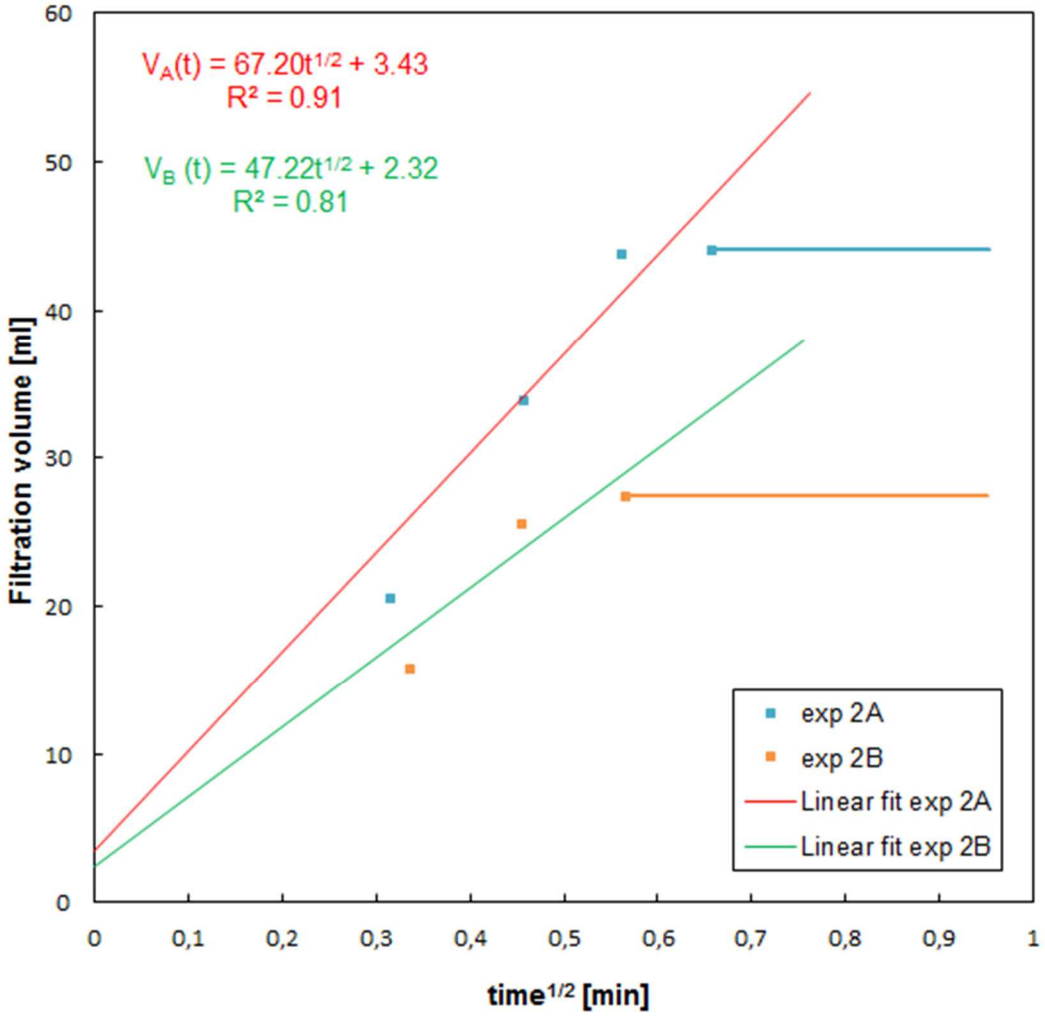

Figure 16: Filtration volume [ml] vs. time [sec] for experiments 2A and 2B. The spurt loss volume is 3.43 ± 0.05 ml and 2.32 ± 0.05 ml for experiment 2A and 2B respectively.

5.2.3 External filter cake and internal filtration characterisation

Due to limitations of the scanning electron microscope it was not possible to use this device to make images of the external filter cake and internal filtration. The external filter cake had a thickness of 35.0 ± 0.5 mm (Figure 17). The homogenous consistency of this external filter cake shows great similarity with the one from experiment 1A (Figure 11). This resemblance in combination with the fast leak-off rate, leads to the conclusion that the external filter cake has a poor packed construction as seen on the images from experiment 1 (Figure 12). Together with the observed homogeneous content of the filter cake, this leads to the statement that the main component of the external filter cake is calcium carbonate. The characterisation of the internal filtration without the scanning electron microscope is not possible.

Figure 17: Top part of the core of experiment 2A, external filter cake is 35 ± 0.5 mm

5.3 Leak-off into Brine Saturated Core

5.3.1 CT scan images and attenuation profiles

Experiment 3 is executed with the same drilling fluid composition (Table 1) and the core initially saturated with 3.5 wt% NaCl brine. Figure 18 shows the CT scan images at different times. The start image clearly shows external filter cake formation immediately after pressurizing the system. This is in agreement with the results from experiment 2. From 6 seconds onwards a very rapid build-up of external filter cake is observed, also similar to the process in experiment 2. The experiment was run until all the drilling fluid is finished; contributing to the external filter cake build-up or filtering into the core. This occurs after 46 seconds which is a longer time than encountered in the oil saturated core, because of the larger drilling fluid start volume. Two phase flow in the core slows down the leak-off, as shown from the external filter cake thickness obtained at 12s for both experiments. However the leak-off rate for both the experiments due to the high permeability of the core. A total of 18 CT scan images were shot in a time span of 13 minutes. The corresponding attenuation profiles are displayed in Figure 19. This figure includes the attenuation profile of the CT scan image of the core holder and core without the drilling fluid on top (middle vertical blue line). After the drilling fluid is finished, the attenuation profiles show a lower value for the external filter cake. This was also observed in experiment 2 due to penetration of air.

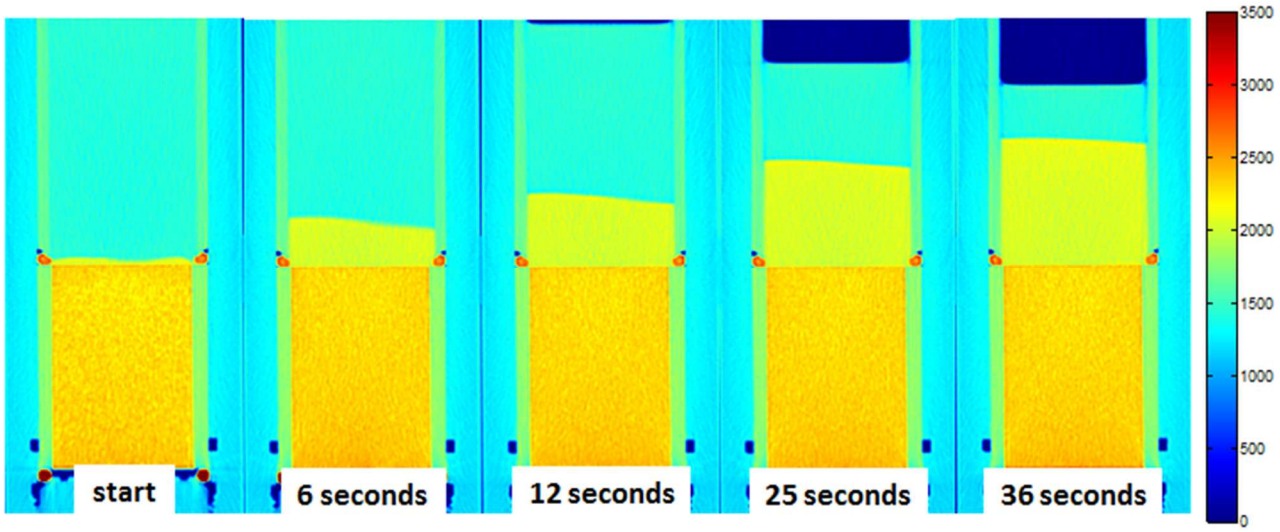

Figure 18: CT scan images of experiment 3A at different times, visualising the leak-off process and used to construct the attenuation profiles.

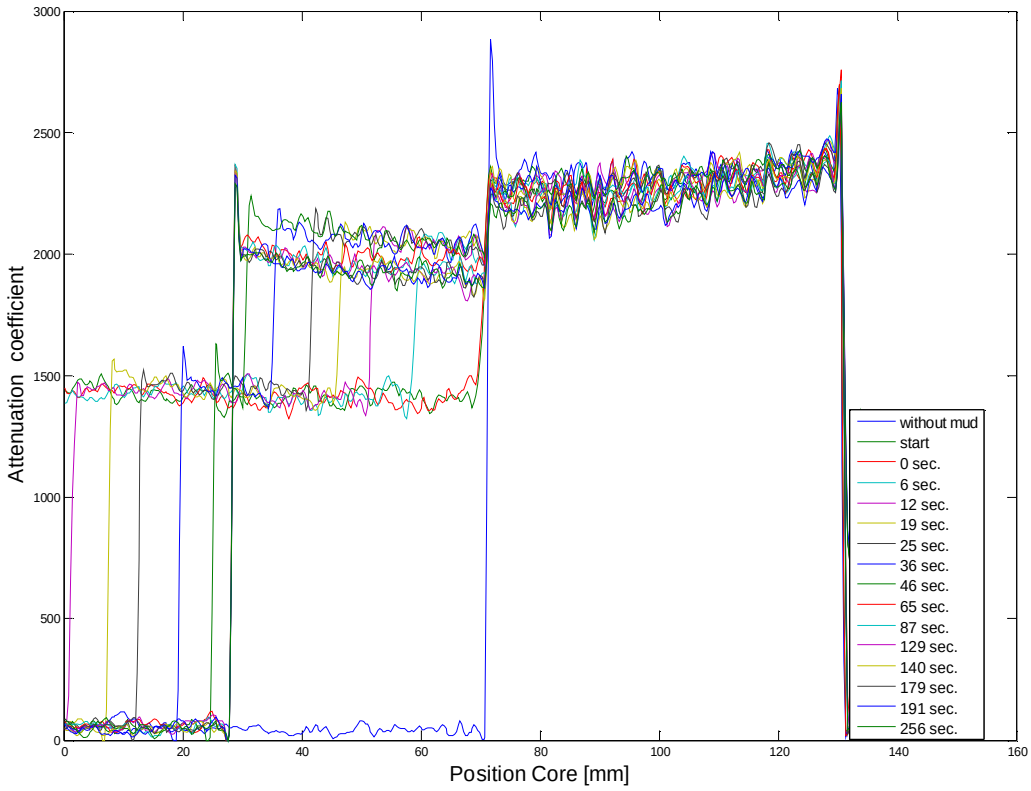

Figure 19: Attenuation profiles for experiment 3A at different times, created with CT scan images, used to determine the leak-off volume. The outstanding vertical blue line in the middle represents a CT scan image of the saturated core, without the drilling fluid on top.

5.3.2 Leak-off volume

Figure 20 presents the leak-off volume as a function of the square root of time for experiments 3A and 3B and the corresponding fitted models. This linear fit is plotted through the first 6 (3A) and 4 (3B) data points up until where the drilling fluid is finished (solid lines). The model fit for experiment 3B is good and the fit for experiment 3A is fairly good. The found spurt volumes were 1.06 ± 0.05 ml and 2.93 ± 0.05 ml for experiments A and B respectively. These values are less than the highest spurt loss found in experiments 2A and 2B. The leak-off rates are also lower than encountered in experiment 2. This is as expected due to the two-phase flow in the core and drilling fluid composition and core permeability kept the same. The effluent as a result of the leak-off process first consisted of brine, later both oil (from the drilling fluid) and brine and in the end only oil. The effluent volumes were 70 ± 0.5 ml and 68 ± 0.5 ml for experiment 3A and 3B respectively both containing 10 ± 0.5 ml brine. Comparing with the total leak-off volumes of 44 ± 0.5 ml and 42 ± 0.5 ml respectively

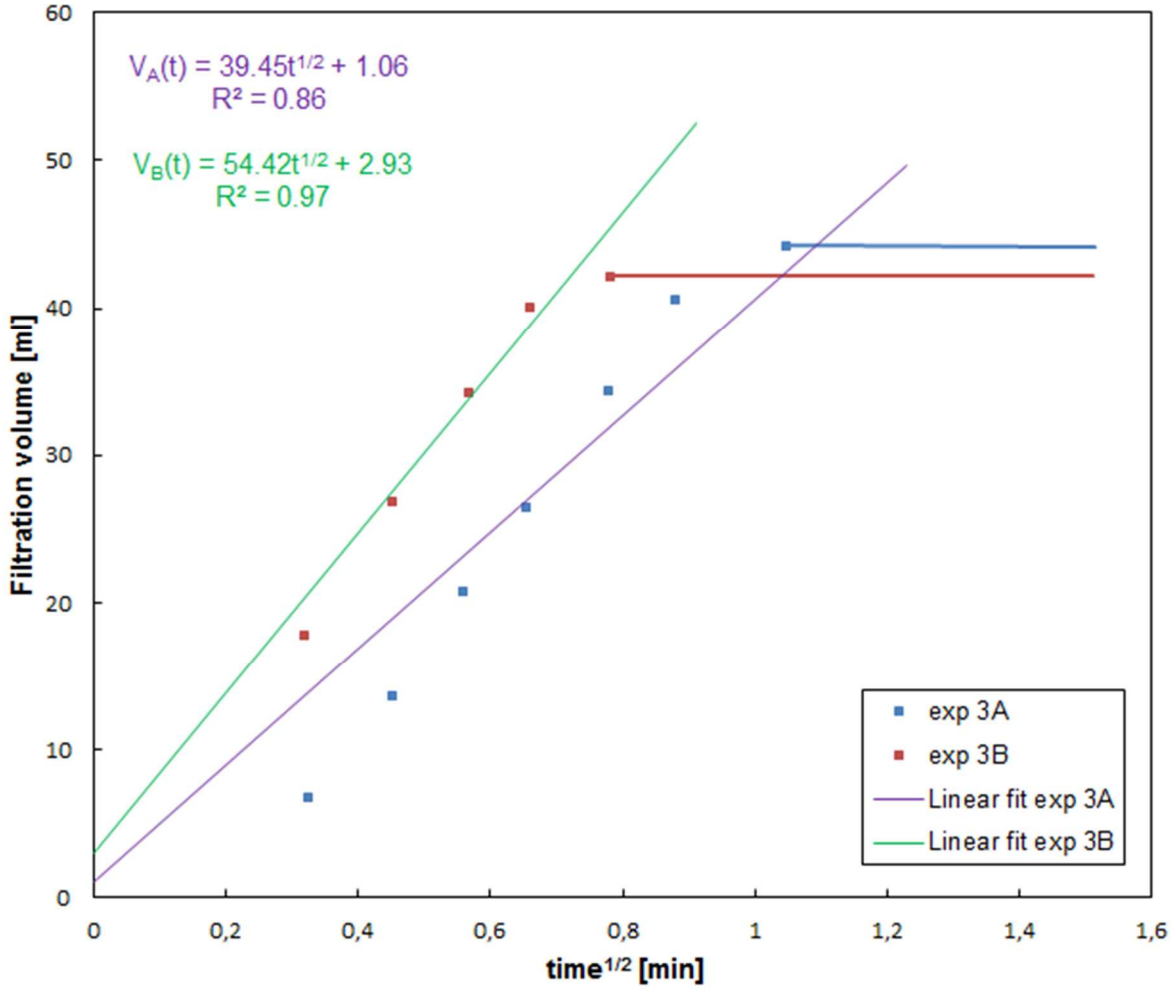

Figure 20: Filtration volume [ml] vs. time [sec] for experiments 3A and 3B. The spurt loss volume is 1.06 ± 0.05 ml and 2.93 ± 0.05 ml for experiment 3A and 3B respectively.

5.3.3 External filter cake and internal filtration characterisation

The external filter cake has a thickness of approximately 49.0 ± 0.5 mm (Figure 21). Figure 22 shows part of this external filter cake together with images of the internal filtration of the particles into the core. The particles have a sharp-edged shape. The images show large interconnected pores which could explain the high permeability observed in the core. The larger image of the internal filtration shows that small calcium carbonate particles penetrate at least 1 cm into the core. This could not be detected by the CT scanner however, due to the low difference of CT attenuation coefficient of calcium carbonate compared to sandstone. It is also observed that not all the space in between the grains is filled with particles from the drilling fluid. The last image shows that calcium carbonate particles not only tend to form aggregates, but they also stick onto the grains surfaces. However, the particles do not form a sealing layer. The lack of sealing can be explained by the sharp-edged shape of the particles rather than a round shape. The particles do not form a dense packing and therefore porosity and permeability stay high, leaving space for drilling fluid and particles to pass through.

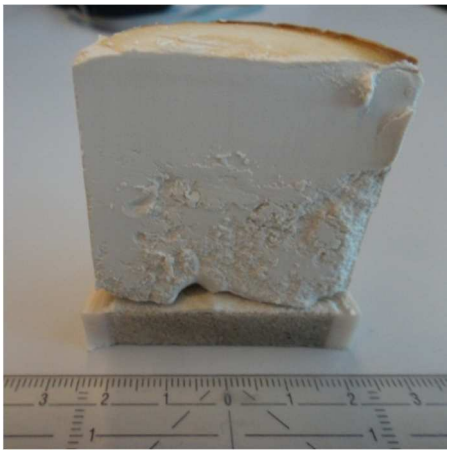

Figure 21: Top part of the core of experiment 3A, used for ESEM characterisation and external filter cake (49 ± 0.5 mm)

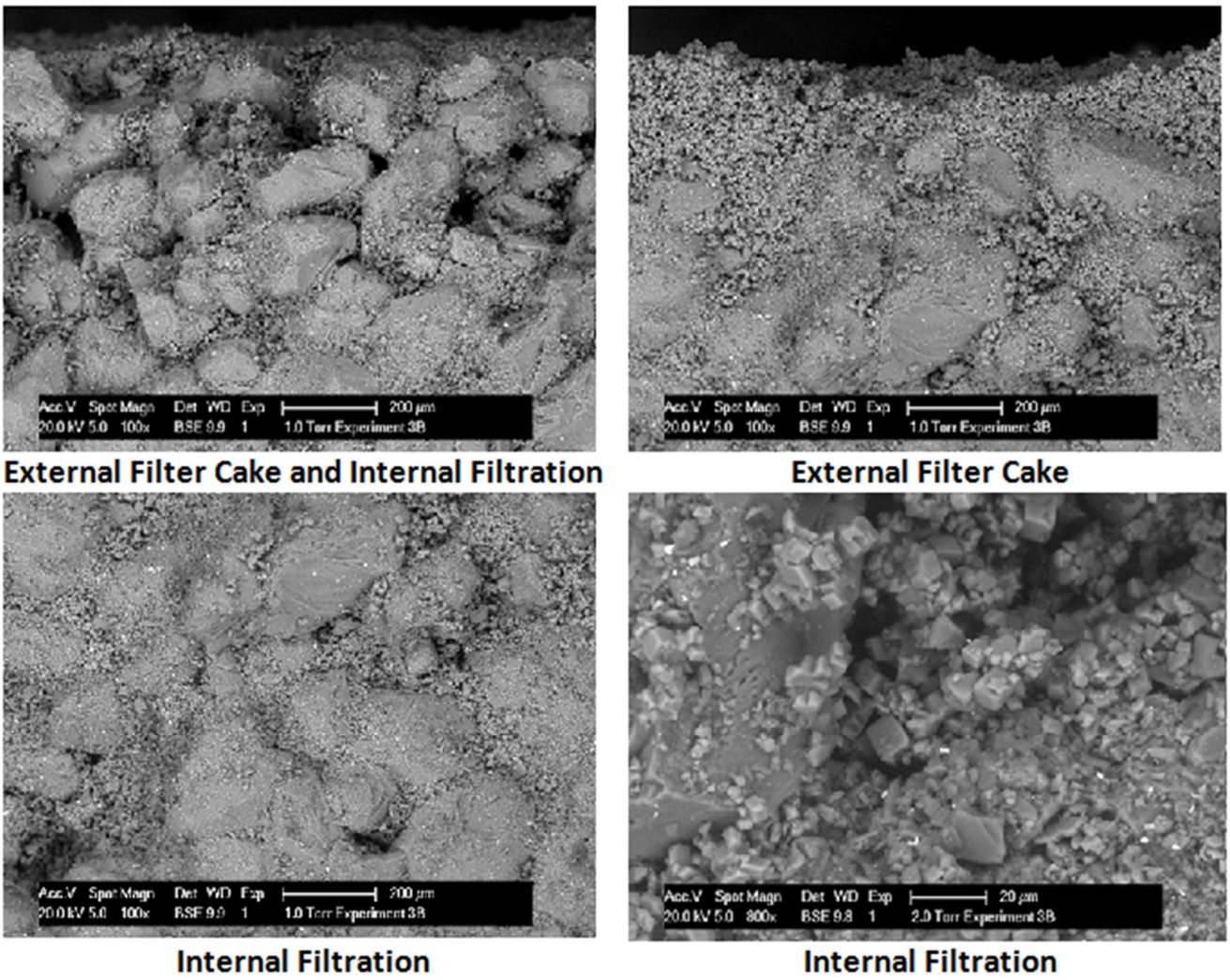

Figure 22: Images of external filter cake and internal filtration for experiment 3A, obtained by ESEM

Figure 23 shows the elemental analysis for the external filter cake and the internal filtration for experiment 3A. The marker elements for the particles used in the drilling fluid are displayed in Table 6. Calcium carbonate, bentonite and lime penetrate into the core. The external filter cake contains the largest part of the calcium carbonate.

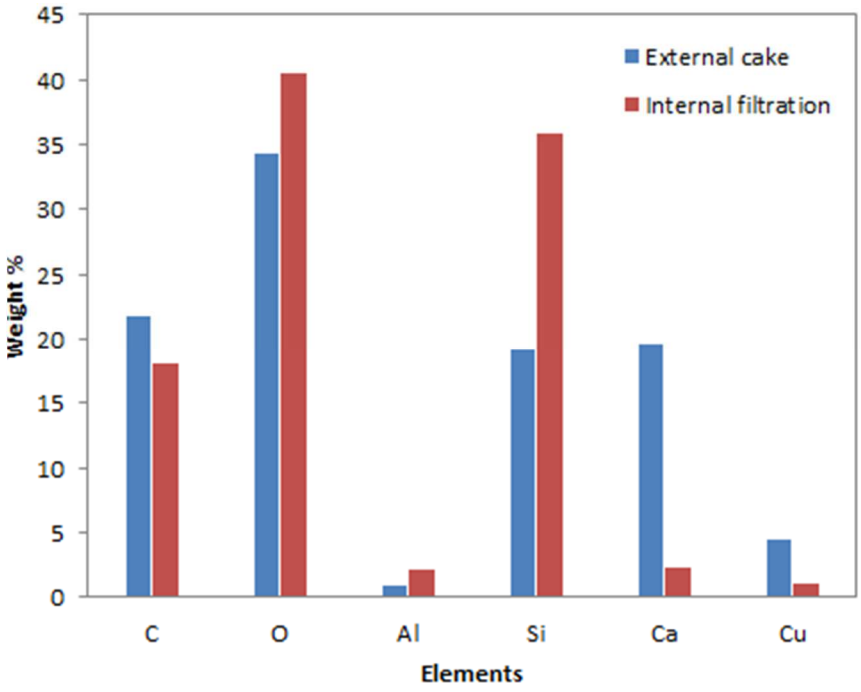

Figure 23: Elemental analysis for external cake and internal filtration of experiment 3A, obtained by EDAX. The elements are displayed in weight %

5.4 Leak-off of Barite Drilling Fluid into Brine Saturated Core

To verify that the results from experiments 2 and 3 are caused by addition of calcium carbonate and not due to the saturation of the cores experiment 4 (Table 5) is executed. For this experiment the main component in the drilling fluid is changed to barite, preserving the same volume percentage. An overview of the results is found in Appendix III, in total 23 images were shot in 41 minutes.

The X-ray attenuation coefficient of barite is very large. Therefore the CT scan images present pronounced streak artefacts. The images cannot be used because they contain too much noise and therefore might give an inaccurate picture of the leak-off process. The ESEM images in Figure 24 are used to confirm the suggested statements on particle size differences and particle shape. From the barite images it is clear that the occurrence of different particle sizes and shapes contributes to the formation of a dense external filter cake. The small particles fill up the gaps left by the larger particles. The low value of effluent (2.8 ± 0.1 ml) confirms that the composition of the filter cake prevents the severe and quick leak-off encountered in experiments 2 and 3.

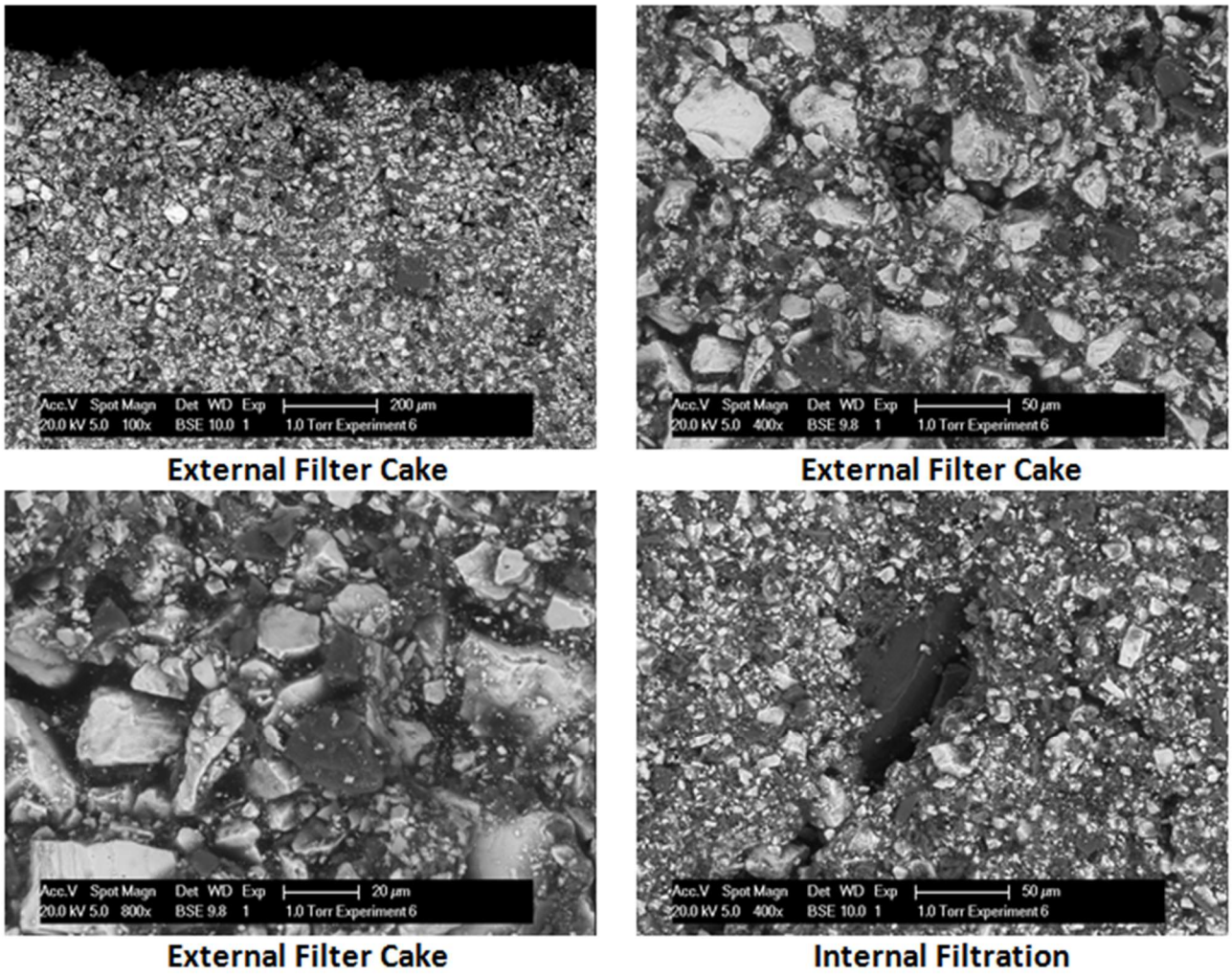

Figure 24: ESEM images of external filter cake and internal filtration of experiment 4

5.5 Brine Saturated Core and Hematite Drilling Fluid

5.5.1 CT scans and attenuation profiles

The experiments presented above with calcium carbonate drilling fluid d_{50} = 14 ± 1 mm (experiments 1 through 3) showed fairly rapid leak-off rates. This is primarily due to a high permeability of the external filter cake. In an attempt to create a less permeable filter cake hematite with a d_{50} of 5 µm was used in the drilling fluid instead of the calcium carbonate. A brine saturated core was used to enable comparison with experiment 3 and the use of ESEM analysis. Figure 25 shows CT scan images representing the leak-off process of experiment 5, in total 22 images were shot over a time span of 45 minutes. The drilling fluid attenuation coefficient is higher than for calcium carbonate experiments but it is lower than the barite drilling fluid. This is caused by the change in main component in the drilling fluid which has an intermediate X-ray response compared to previous used components. The start image shows no internal filtration and a small external filter cake like the start image of experiment 3, where also immediate particle deposition on the interface between the drilling fluid and the core was distinguished. After 6 seconds internal filtration is visible. The colour change inside the core after 7 and 29 minutes suggest hematite particles travelling through the core before being deposited. This is more clearly visible in the attenuation profiles displayed in

Figure 26. The external filter cake build-up from the start onwards is significantly slower than the cake build-up in experiments 2 and 3. The dark red colour suggests that the main component of the filter cake is hematite, this was verified with the external filter cake characterisation as discussed below. The small yellow colour changes at the top of the drilling fluid can be some small air bubbles. This air could have penetrated the mud during filling of the syringe used for the drilling fluid injection. The red line at the air-drilling fluid interface suggests a hematite layer at the top of the drilling fluid. This is strange as hematite has a high specific gravity and is therefore not likely to float on top. In the attenuation profiles this is also observed, after the air-drilling fluid interface the profiles take some time to merge to a stable value. This is different than seen from the profiles of experiment 2 and 3. The high attenuation coefficient of the external filter cake also differs, this is due to the change in drilling fluid component.

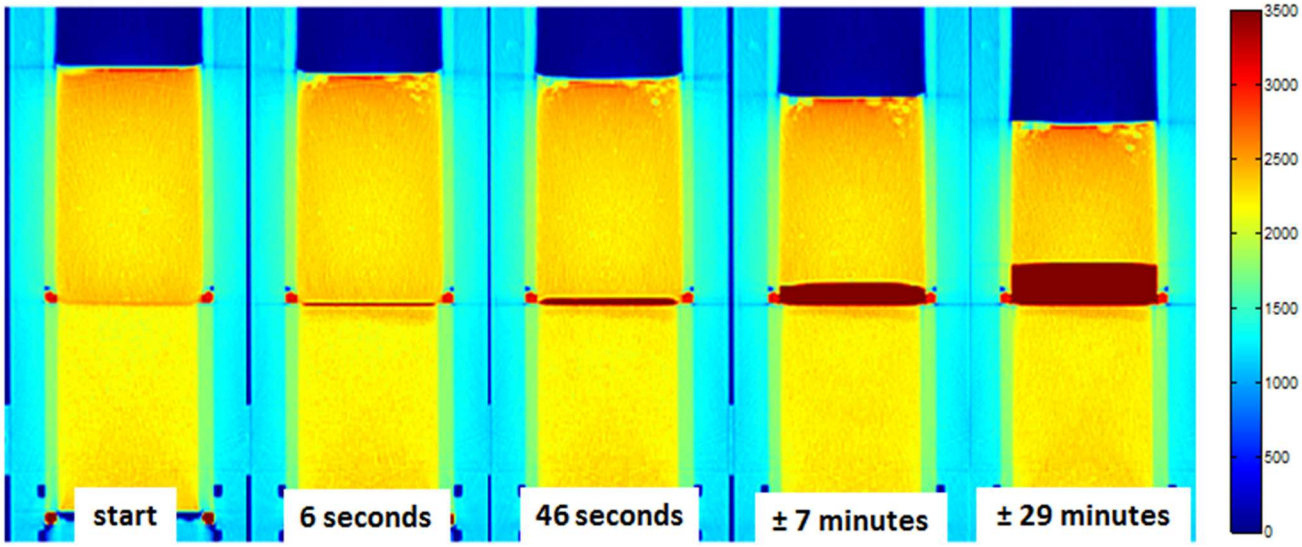

Figure 25: CT scan images of experiment 5A at different times, visualising the leak-off process and used to construct the attenuation profiles.

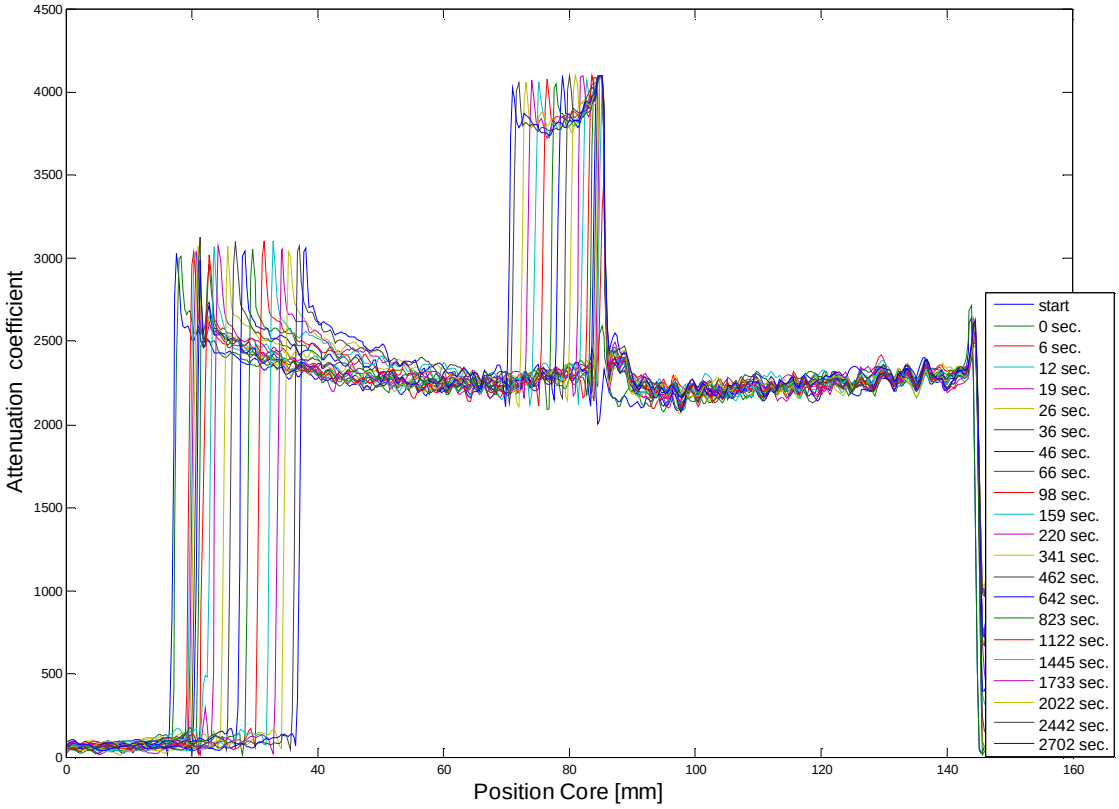

Figure 26: Attenuation profiles for experiment 5A at different times, created with CT scan images, used to determine the leak-off volume. Notice the larger spacing between the 0 seconds curve and the 6 seconds curve on the left of the graph, indicating the spurt loss.

5.5.2 Leak-off volume

Figure 27 shows plots of the filtration volume for experiments 5A and 5B as a function of the square root of time. Curves show a spurt loss volume 1.09 ± 0.05 ml and 0.53 ± 0.05 ml, respectively, found by extrapolating the fitted line. Although the spurt loss volume is small for both experiments, the leak-off after 45 minutes (22.49 ± 0.05 ml and 24.02 ± 0.05 ml) is higher than the leak-off volume encountered in the dry core experiments (5.1). The curves show good reproducibility similarly to experiments 1A and 1B and they are in agreement with the presented theory. However, the leak-off is smaller than for experiment 3. These observations are supported by comparison of the volume of the effluent: these are 17 ± 0.5 and 24 ± 0.5 ml for experiment 5A and 5B respectively. The volumes of brine in the effluent were 5 ± 0.5 and 6 ± 0.5 ml for 5A and 5B respectively. The difference in total effluent volume can be explained by the longer run time of experiment 5B, the experiment ran 15 minutes longer than experiment 5A. The difference in total leak-off volume (22 ± 0.05 ml for 5A and 28 ± 0.05 ml for 5B) is compatible with the difference in effluent volumes. The effluent volumes do not comprise both the leak-off volume and the pore volume which suggest not all the leaked-off drilling fluid is pushed entirely through the core (no total breakthrough). This is confirmed by the volumes of brine in the effluent compared to the volume of brine in the effluents of experiment 3 (10 ± 0.5 ml). This is plausible because unlike in experiment 3 not all the drilling fluid is finished so there will still be some leaked-off fluid in the core as well. In Figure 28 the effluents (in grams) are plotted as a function of time. The course of both curves is similar except for the almost stable part of the curve for experiment 5B. The steep starts corresponds to the spurt loss, then the effluent curve for 5A continues at a steep rate to

slow down production with time, more than the curve for 5B. This can be explained by the higher leak-off rate of experiment 5B after the spurt loss (Figure 27). The steady part of curve 5B is quite remarkable but can partly be explained by the slow start of the leak-off compared to experiment 5A.

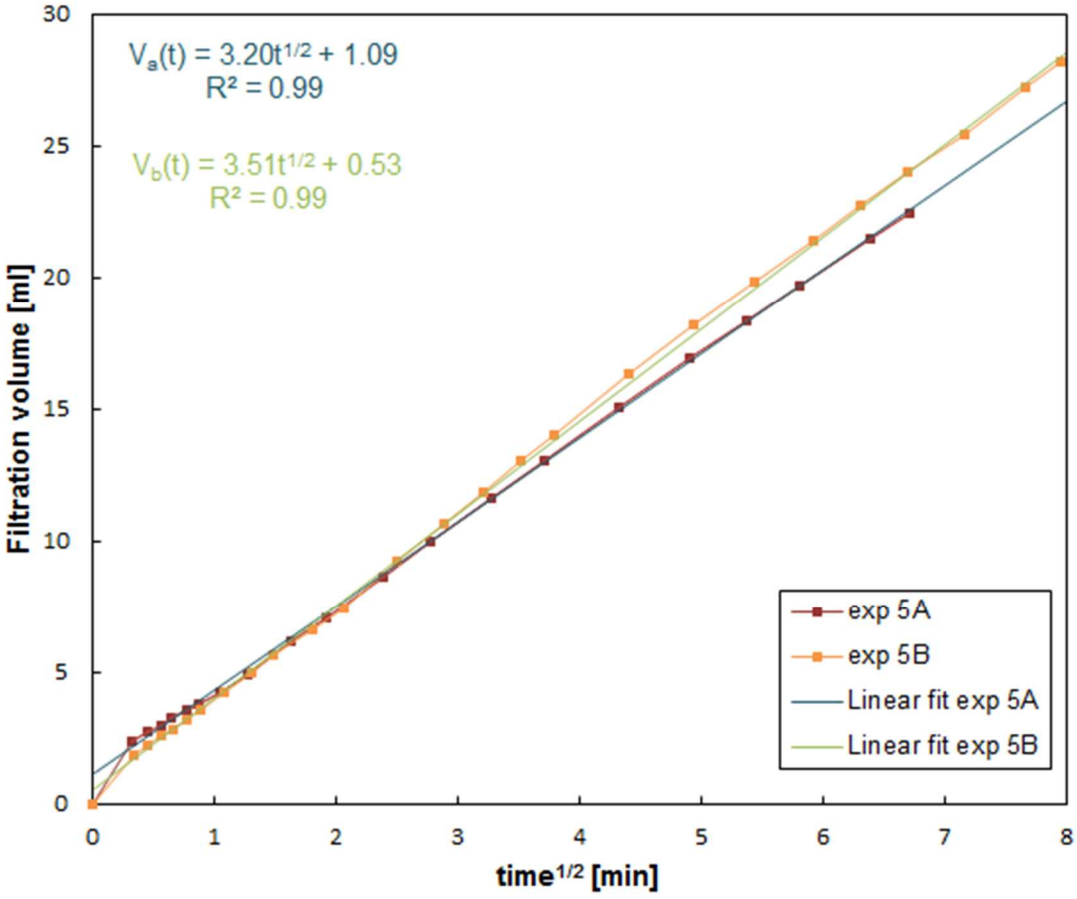

Figure 27: Filtration volume [ml] vs. the square root of time [min] for experiments 5A and 5B. The spurt loss volume is 1.09 ± 0.05 ml and 0.53 ± 0.05 ml for experiment 5A and 5B respectively.

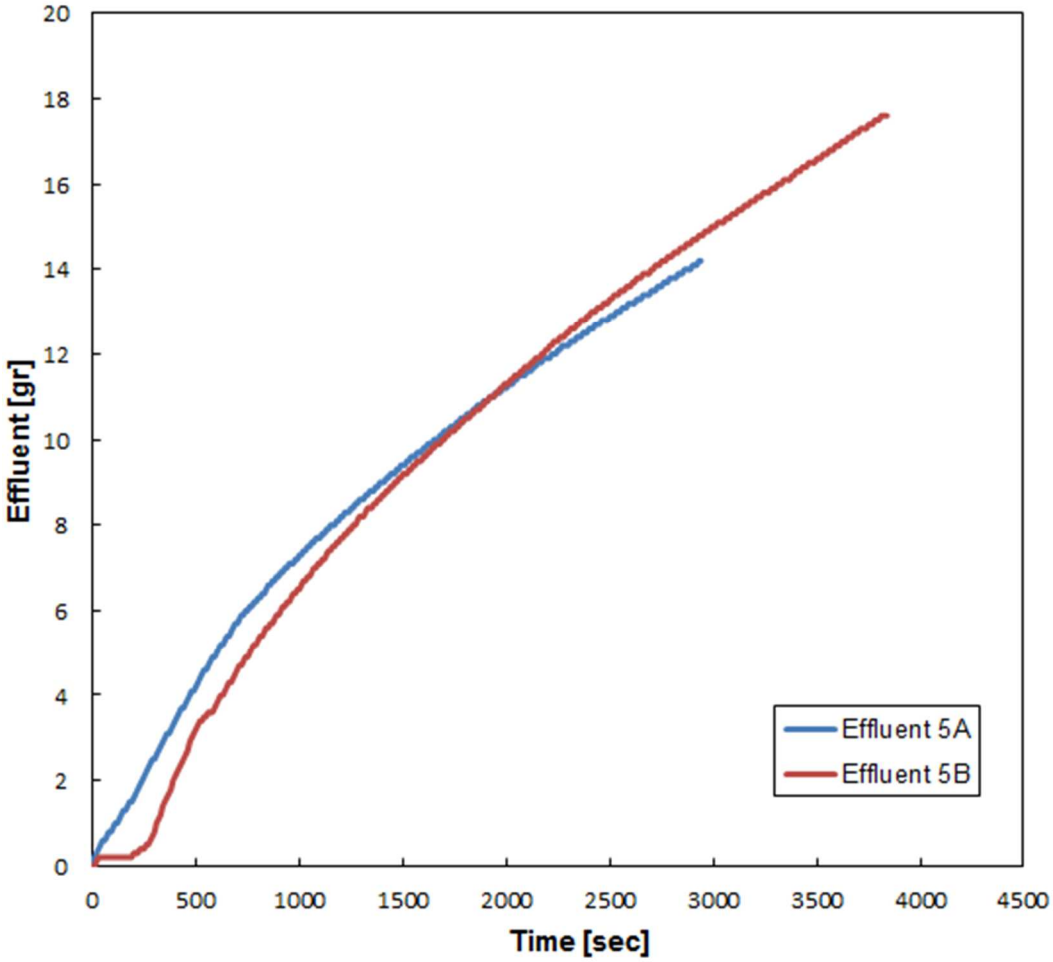

Figure 28: Effluent [gr] as a function of time [sec] for experiment 5A and 5B. The crossing of the curves can be explained by the difference in leak-off rate after the spurt time.

5.5.3 External filter cake and internal filtration characterisation

The external filter cake has a thickness of 17 ± 0.5 mm (Figure 29), which is a lot smaller than the found thickness of the calcium carbonate external filter cake. This can be explained by the lower permeability hematite external filter cake in Figure 30. The leak-off of drilling fluid is less which results in a thinner external filter cake. From the internal images it is seen that the pore space is filled up with a large amount of particles, more than in the case with calcium carbonate. This can be explained by the size difference between the particles. The size of the hematite particles is smaller leading to more efficient blocking of the pore space. The hematite particles are round-shaped rather than sharp-edged enabling a more efficient packing in the pore space. Both leading to a larger reduction of permeability in the core compared to experiment 3.

Figure 29: Top part of the core and external filter cake (17 ± 0.5 mm)

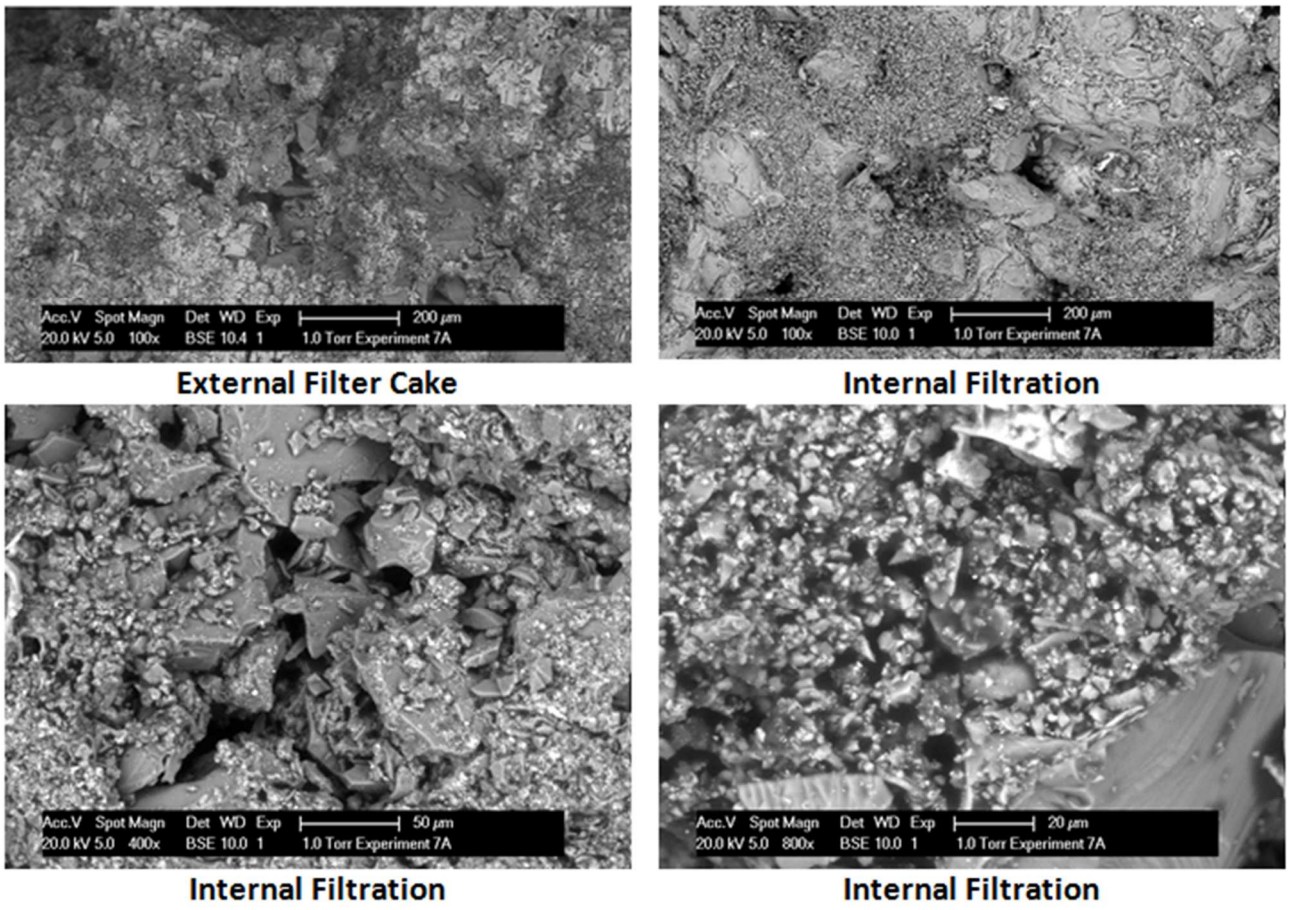

Figure 30: ESEM images from external filter cake and the top of the core from experiment 5A

6. Conclusions & Recommendations

6.1 Conclusions

Static leak-off experiments with oil-based drilling fluid were performed into both dry and liquid-saturated cores. The drilling fluid's main components were either calcium carbonate or hematite. The set-up was positioned in a CT scanner to follow the leak-off process. The experimental data was fitted to the developed model for saturated cores. An ESEM analysis was performed to characterize the external filter cake and internal filtration.

From the performed experiments and the presented work the following conclusions can be drawn:

- Spurt loss and leak-off volume for a calcium carbonate oil-based drilling fluid are less in a dry core than in either oil- or brine saturated cores. The leak-off into oil saturated cores is the fastest, in brine saturated cores the two-phase flow slows down the leak-off rate to some extent.
- Calcium carbonate particles are less effective in leak-off control than barite particles in brine saturated cores. A suggested explanation is the shape and clogging effect of the particles resulting in a higher permeable calcium carbonate filter cake versus the barite filter cake.
- Spurt loss and leak-off volume for a hematite oil-based drilling fluid are significantly less than for a calcium carbonate oil-based drilling fluid in brine saturated cores. For the hematite drilling fluid not all the brine was pushed out of the core.
- Larger calcium carbonate particles are less effective in leak-off control than smaller sized hematite particles in brine saturated core. The hematite particles show a denser packing, blocking the pores more effectively, creating a less permeable filter cake and a dense internal filtration.
- The sharp-edged shape and the size of the calcium carbonate particles result in a loose packing of the particles which causes a permeable external filter cake and a wide spread internal deposition. The lack in difference of particle sizes prevents the smaller space between grains and particles to be filled, leaving space for the drilling fluid to pass through.
- The more rounded-shape of hematite particles makes them more efficient in blocking the pore space compared to the rectangular shaped calcium carbonate particles.
- Different particle sizes in the barite filter cake are an important factor in producing a low permeable filter cake, where smaller particles fill up the gaps between the large particles.
- Permeability difference between the cores made it difficult to compare the dry core experiment results with previous work

6.2 Recommendations

The experiments performed in this study were static filtration experiments. These are not influenced by erosion and compaction resulting from flow. The effect of flow was therefore not taken into account in this study. In addition, the statements on the filter cake were derived from ESEM analysis only. To complete the conclusions on the role of particle sizes and shapes, particle distributions are important to add.

For further research on this topic a few recommendations are suggested:

- To extend the knowledge of the influence of brine- and oil saturation, a systematic study with varying saturations should be performed
- To get a better understanding of the influence of the particle size, investigation of more different particles sizes and the mixing of these sizes in drilling fluid is necessary. The particle sizes should be carefully selected and distributions should be available.
- For the formation of a sealing external filter cake, it is suggested to use different particle sizes in the drilling fluid.
- Small scale dynamic filtration tests with the same drilling fluids used in this work can highlight differences between the static and dynamic process.
- A next step in translating the conducted laboratory experiments to the field is up-scaling the experiments to verify the results for larger cross sectional areas.

Nomenclature

a = Klein-Nishina coefficient

c = concentration of suspended particles

c_p = concentration of particles in fluid

c_1 = concentration of particles in external filter cake

c_2 = concentration of particles in internal filtration

C = total concentration of particles

D = dispersion coefficient

E = photon energy

$\overline{f_o}(w)$ = average fractional flow of oil in brine saturated medium

k = permeability of the core

k_c = permeability of external filter cake

$k_{ro}(s_{wc})$ = relative oil permeability at connate water saturation

L = length of the core

l_c = length of external filter cake

l_{ow} = length of top of core to oil-water interface

ΔP_c = pressure drop over external filter cake

ΔP_{core} = pressure drop over the core

S = cross sectional area of core

S_o^0 = initial oil saturation

S_w^0 = initial water saturation

S_{wc} = connate water saturation

$\bar{S}_{w(t)}$ = average water saturation

t = time

t_s = spurt loss time

u = velocity

v = interstitial velocity

V = total drilling fluid volume

V_p^{fc} = volume of particle trapped in external filter cake

V_p^{pm} = volume of particles penetrating the porous medium

V_s = spurt loss volume

$V(t)$ = filtration volume

z = distance along the core in flow direction

Z = effective atom number

η_o = viscosity of oil

η_w = viscosity of water

λ = filtration coefficient

μ = linear attenuation coefficient

ρ = electron density

σ = concentration of deposited particles

ϕ = porosity of the core

ϕ_c = porosity of external filter cake

References

Al-Abduwani, F. A. H., Farajzadeh, R., van den Broek, W. M. G. T., Currie, P. K. & Zitha, P. L. J. (2005). *Filtration of Micron-Sized Particles in Granular Media Revealed by X-Ray Computed Tomography*. Review of Scientific Instruments*, 76*(103704), 6. doi: 10.1063/1.2103467

Al-Abduwani, F. A. H., Shirzadi, A., van den Broek, W. M. G. T. & Currie, P. K. (2005). *Formation Damage vs. Solid Particles Depostion Profile During Laboratory-Simulated Produced-Water Reinjection*. SPE Journal*, June 2005*, 138-151.

Al-Riyamy, K. & Sharma, M. M. (2004). *Filtration Properties of Oil-in-Water Emulsions Containing Solids*. SPE Drilling & Completion, 164-172. doi: 10.2118/73769-MS

Aston, M., Mihalik, P. & Tunbridge, J. (2002). *Towards Zero Fluid Loss Oil Based Muds*. Paper presented at the SPE Annual Technical Conference and Exhibition, San Antonio, Texas. 29 September-2 October

Bailey, L., Boek, E. S., Jacques, S. D. M., Boassen, T., Selle, O. M., Argillier, J.-F. & Longeron, D. G. (2000). *Particulate Invasion From Drilling Fluids*. SPE Journal*, 5*(4), 412-419. doi: 10.2118/67853-PA

Bedrikovetsky, P., Marchesin, A., Shecaira, F., Souza, A. L., Milanez, P. V. & Rezende, E. (2001). *Characterisation of Deep Bed Filtration System From Laboratory Pressure Drop Measurements*. Journal of Petroleum Science and Engineering*, 32*(2-4), 167-177.

Bedrikovetsky, P., Marchesin, D., Hime, G., Siqueira, A. G., Serra, A. L., Rodrigues, J. R. P., . . . Vinicius, M. (2004). *Inverse Problems for Treatment of Laboratory Data on Injectivity Impairment*. Paper presented at the SPE International Symposium and Exhibition on Formation Damage Control, Lafayette, Louisiana, USA. 18-20 February

Bedrikovetsky, P., Tran, T. K., van den Broek, W. M. G. T., Marchesin, D., Rezende, E., Siqueira, A., . . . Shecaira, F. (2003). *Damage Characterisation of Deep Bed Filtration From Pressure Measurements*. SPE Production & Facilities*, 18*(2), 119-128. doi: 10.2118/83673-PA

de Blok, G. L. J. (May 2012), private communication

Bourgoyne, A. T., Jr, Millheim, K. K., Chenevert, M. E. & Young, F. S., Jr. (1991). *Applied Drilling Engineering* (Vol. 2; SPE Textbook Series).

Byrne, M. T., Spark, I. S. C., Patey, I. T. M. & Twynam, A. J. (2000). *A Laboratory Drilling Mud Overbalance Formation Damage Study Utilising Cryogenic SEM Techniques*. Paper presented at the SPE International Symposium on Formation Damage Control, Lafayette, Louisiana. 23-24 February

Civan, F. (1994). *A Multi-Phase Mud Filtrate Invasion and Wellbore Filter Cake Formation Model*. Paper presented at the SPE International Petroleum Conference & Exhibition of Mexico, Veracruz, Mexico. 10-13 October

Clark, P. E. & Barkat, O. (1990). *Analysis of Fluid-Loss Data*. SPE Production Engineering*, 5*(3), 306-310. doi: 10.2118/18971-PA

Cobianco, S., Bartosek, M., Lezzi, A. & Guarneri, A. (2001). *How To Manage Drill-In Fluid Composition To Minimize Fluid Losses During Drilling Operations*. SPE Drilling & Completion, 154-158.

Hannegan, D., & Fisher, K. (2005). *Managed Pressure Drilling in Marine Environments.* Paper presented at the International Petroleum Technology Conference, Doha, Qatar. 21-23 November

Herzhaft, B., Audibert-Hayet, A., Sandford, R. & Freche, P. (2001). *Optimization of SBM Formulations for Minimum Damage*. Paper presented at the SPE International Symposium on Oilfield Chemistry, Houston, Texas, USA. 13-16 February

Herzig, J. P., Leclerc, D. M. & Le Goff, P. (1970). *Flow of Suspensions through Porous Media - Application to Deep Filtration*. Industrial and Engineering Chemistry*, 62*(5), 8-35.

Hua, G., Vonken, J. & Zitha, P. L. J. (2010). *Feasibility Study of the Mitigation of Loss Circulation in Oil-Based Drilling Fluids Using Gilsonite.* Delft University of Technology, Delft. (Internal Report)

Iwasaki, T. (1937). *Some Notes on Sand Filtration*. Journal of the American Water Works Association*, 29*, 1591-1602.

Kelessidis, V. C., Marinakis, D. & Tsamantaki, C. (2007). *Laboratory Assessment of Drilling-Fluid Formation Damage in Sandstone Cores and Mitigation With Lignite Additives for High-Temperature Fields*. Paper presented at the European Formation Damage Conference, Scheveningen, The Netherlands. 30 May-1 June

Liu, X. & Civan, F. (1996). *Formation Damage and Filter Cake Buildup in Laboratory Core Tests: Modeling and Model-Assisted Analysis*. SPE Formation Evaluation, 26-30.

Lord, D. L., Vinod, P. S., Shah, S. N. & Bishop, M. L. (1998). *An Investigation of Fluid Leakoff Phenomena by Use of a High-Pressure Simulator*. SPE Production & Facilities*, 13*(4), 250-257. doi: 10.2118/52394-PA

McCullough, E. C. (1975). *Photon Attenuation in Computed Tomography*. Medical Physics*, 2*(6), 307-320.

Navarrete, R. C., Dearing, H. L., Constien, V. G., Marsaglia, K. M., Seheult, J. M. & Rodgers, P. E. (2000). *Experiments in Fluid Loss and Formation Damage with Xanthan-Based Fluids While Drilling*. Paper presented at the IADC/SPE Asia Pacific Drilling Technology, Kuala Lumpur, Malaysia. 11-13 September

Nunes, M., Bedrikovetsky, P., Newbery, B., Paiva, R., Furtado, C. & de Souza, A. L. (2010). *Theoretical Definition of Formation Damage Zone With Applications to Well Stimulation*. Journal of Energy Resources Technology*, 132*(033101), 1-7.

Pang, S. & Sharma, M. M. (1997). *A Model for Predicting Injectivity Decline in Water-Injection Wells*. Paper presented at the SPE Annual Technical Conference and Exhibition, New Orleans. 25-28 September

Rojas, J. C., Bern, P. A., Fitzgerald, B. L., Modl, S. & Bezant, P. N. (1998). *Minimising Down Hole Mud Losses*. Paper presented at the 1998 IADC/SPE Drilling Conference, Dallas, USA.

Romero, S. N., Monroy, R. R., Johnson, C., Cardenas, F. & Abraham, G. A. T. (2006). *Preventing Lost Circulation by Use of Lightweight Slurries With Reticular Systems: Depleted Reservoirs in Southern Mexico*. SPE Drilling & Completion*, 21*(3), 185-192. doi: 10.2118/92187-PA

Roque, C., Chauveteau, G., Renard, M., Thibault, G., Bouteca, M. & Rochon, J. (1995). *Mechanisms of Formation Damage by Retention of Particles Suspended in Injection Water*. Paper presented at the European Formation Damage Conference, The Hague, The Netherlands. 15-16 May

Saasen, A., Omland, T. H., Ekrene, S., Brévière, J., Villard, E., Kaageson-Loe, N., . . . Meeten, G. (2009). *Automatic Measurement of Drilling Fluid and Drill-Cuttings Properties.* SPE Drilling & Completion, *24*(4), 611-625. doi: 10.2118/112687-PA

Saraf, A., de Zwart, A. H. & Currie, P. K. (2010). *Analysis of the Effect of Residual Oil on Particle Trapping During Produced-Water Reinjection Using X-Ray Tomography*. SPE Journal*, December 2010*, 949-957.

Sharma, M. M. & Yortsos, Y. C. (1987). *Transport of Particulate Suspension in Porous Media: Model Formulation*. AlChE Journal*, 33*(10), 1636-1643.

Tare, U. A., Whitfill, D. L. & Mody, F. K. (2001). *Drilling Fluid Losses and Gains; Case Histories and Practical Solutions*. Paper presented at the 2001 SPE Annual Technical Conference and Exhibition, New Orleans, Louisiana. 30 September-3 October

van Overveldt, A. S. (2011). *A CT Scan Aided Core-Flood Study of the Leak-Off Process in Oil-Based Drilling Fluids.* MSc, Delft University of Technology, Delft. (AES/PE/11-14)

Vinegar, H. J. & Wellington, S. L. (1986). *Tomographic Imaging of Three-Phase Flow Experiments*. Review of Scientific Instruments*, 58*(1), 96-107. doi: 0034-6748/87/010096-12

Walker, B. H. & Black, A. D. (1993). *Dynamic Spurt-Loss Beneath an Oilfield Bit*. Paper presented at the 1993 SPE/IADC Drilling Conference, Amsterdam, The Netherlands. 23-25 February

Appendix

Appendix I: Theoretical Model

Appendix II: CT Scanner

Appendix III: Experimental Results

Appendix I: Theoretical Model

Linear Filtration

The problem geometry is shown schematically in Figure I - 1. Drilling fluid containing suspended solid particles with concentration c_p overlays a porous medium with length L, porosity ϕ and permeability k. Leak-off occurs upon applying a pressure drop ΔP. An external filter cake with thickness l_c, porosity ϕ_c and permeability k_c results on the surface area of the filtration experiment, S.

Mud flowing through the growing external filter cake into the core displaces the fluids initially present in the core. In this study two cases will be considered: a) core is initially at the connate water saturation and b) initially core is fully saturated with brine. In former case a) there will be single-phase flow in both external filter cake and in the core whereas in the latter case flow through the filter cake will be single phase and flow through the porous medium will be two-phase.

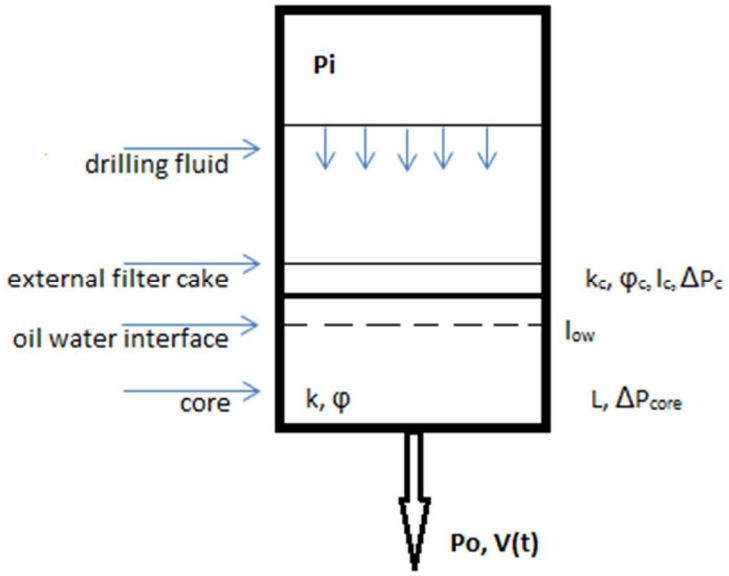

Figure I - 1: Illustration of the model for the external filtration; the drilling fluid is pushed down, penetrating the porous medium, leaving solid particles behind which form the external filter cake. Inside the core the oil-water interface (in case of brine saturated cores) is moving downwards as time is increasing.

Expressions for the leak-off volume were derived for the two subject to the following main assumptions: (1) solid particles and fluids are incompressible, (2) flow is laminar isothermal, (3) only the solid particles in the drilling fluid contribute to the external filter cake build-up, (4) no penetration of particles in core before experiment starts, (5) build-up of external filter cake will occur after a short spurt loss time, (6) single-phase flow through formed filter cake and single or two-phase flow through the porous medium (core).

The extended model for both cases is described below, details of the derivations can be found in Appendix I.

The thickness of the filter-cake l_c is obtained by stating that, by mass conservation, the amount of particles filtered out of the fluid equals the amount of particles deposited in the filter cake at any time t. The flow

through the porous cake and the porous medium obey the classical single and multiphase flow based on mass balance and Darcy's laws.

a) Core at the connate water saturation

As already mentioned, in this case, we are dealing with single-phase flow of the drilling fluid without particles with viscosity η_o through the filter cake and through the core. The core is characterized by a relative permeability $k_{ro}(S_{wc})$ at the connate water saturation S_{wc}.

For the thickness of the external filter cake we get

$$(1-\phi_c)l_c(t)S = \frac{c_p}{1-c_p}V(t) \tag{1}$$

$$l_c(t) = \frac{c_p}{(1-c_p)(1-\phi_c)S}V(t) \tag{2}$$

The flow through the porous cake can be described by Darcy's law

$$Q(t) = \frac{k_c}{\eta_o}S\frac{\Delta P_c}{l_c} \tag{3}$$

Then the pressure over the porous external filter cake will be

$$\Delta P_c = \frac{\eta_o c_p}{k_c S^2(1-c_p)(1-\phi_c)}V(t)\frac{dV(t)}{dt} \tag{4}$$

For the flow inside the porous medium the velocity is equal to

$$V(t) = \phi(1-S_{wc})SL \tag{5}$$

Finally the pressure drop over the total system will be

$$\Delta P_{total} = \Delta P_c + \Delta P_{core} \tag{6}$$

The filtration behavior can be described by:

$$Q_1 = [F_2 V(t) + 1]\frac{dV(t)}{dt} \tag{7}$$

With the constants

$$Q_1 = \frac{k}{\eta_o} S \frac{\Delta P}{L}; \qquad F_2 = \frac{c_p k k_{ro}(S_{wc})}{k_c S(1 - c_p)(1 - \phi_c) L}$$

Integrating the expression for Q_1 with $V(t_s) = V_s$ as initial condition gives for V(t):

$$V(t) = \begin{cases} Q_1 t & t < t_s \\ \dfrac{\sqrt{(F_2 V_s + 1)^2 + 2F_2 Q_1 (t - t_s)} - 1}{F_2} & t > t_s \end{cases} \tag{8}$$

Here V_s is the spurt loss volume of filtrate and t_s is the spurt loss time. When V_s and t_s equal zero, the equation for $t > t_s$ becomes:

$$V(t) = \frac{\sqrt{1 + 2F_2 Q_1 t} - 1}{F_2} \tag{9}$$

When $2F_2Q_1 >> 1$ the above equation can be approximated by:

$$V(t) = \sqrt{\frac{2Q_1 t}{F_2}} \tag{10}$$

Equation 10 shows that for an oil-saturated core the filtrate volume is proportional to the square root of time after the spurt loss time.

b) Fully brine saturated core: piston-like displacement

In this case oil (viscosity η_o) displaces water with viscosity η_w in piston like manner. The initial condition in the core is $S_w^0 = S_w(z, 0) = 1$.

Denoting the time dependent position l_{ow} of the oil/water front the core is at connate water saturation for $0 \leq z \leq l_{ow}$.
For the thickness of the external filter cake we get

$$(1-\phi_c)l_c(t)S = \frac{c_p}{1-c_p}V(t) \tag{11}$$

$$l_c(t) = \frac{c_p}{(1-c_p)(1-\phi_c)S}V(t) \tag{12}$$

The flow through the porous cake can be described by Darcy's law

$$Q(t) = \frac{k_c}{\eta_o}S\frac{\Delta P_c}{l_c} \tag{13}$$

Then the pressure over the porous external filter cake will be

$$\Delta P_c = \frac{\eta_o c_p}{k_c S(1-c_p)(1-\phi_c)}V(t)\frac{dV(t)}{dt} \tag{14}$$

For the flow inside the porous medium an idealised piston like flow is assumed and in that case for the time before breakthrough the velocity in the core is

$$V(t) = \phi(1-S_{wc})Sl_{ow}(t) \tag{15}$$

The pressure drop in the core is described as

$$\Delta P_{core} = \Delta P_{l_{ow}(t)} + \Delta P_{L-l_{ow}(t)} \tag{16}$$

Finally the pressure drop over the total system will be

$$\Delta P_{total} = \Delta P_c + \Delta P_{core} \tag{17}$$

The filtration behaviour can be described by:

$$Q_0 = [F_1 V(t) + 1]\frac{dV(t)}{dt} \tag{18}$$

With the constants:

$$Q_0 = \frac{k}{\eta_w} S \frac{\Delta P}{L}; \qquad F_1 = \left[\frac{\eta_o}{\eta_w k_{ro}(S_{wc})} - 1\right]\frac{1}{\phi(1 - S_{wc})SL} + \frac{\eta_o c k}{\eta_w k_c S(1 - c_p)(1 - \phi_c)L}$$

With Q_0 representing the flow [volume per time] in the saturated core. Integrating with the initial condition $V(t_s) = V_s$ we obtain for $V(t)$:

$$V(t) = \begin{cases} Q_0 t & t < t_s \\ \dfrac{\sqrt{(F_1 V_s + 1)^2 + 2F_1 Q_0 (t - t_s)} - 1}{F_1} & t > t_s \end{cases} \tag{19}$$

When V_s and t_s equal zero, the equation for $t > t_s$ becomes:

$$V(t) = \frac{\sqrt{1 + 2F_1 Q_0 t} - 1}{F_1} \tag{20}$$

When $2F_1Q_0 >> 1$ equation 20 can be approximated as

$$V(t) = \sqrt{\frac{2Q_0 t}{F_1}} \tag{21}$$

Equation 21 shows the square root of time dependency of the filtrate volume after the spurt time.

c) Buckley-Leverett displacement

Now we consider the case where idealised piston-like water displacement by oil does not occur. This is done replacing the assumption of idealised piston-like flow behaviour for the two-phase flow in the porous

medium by the Buckley-Leverett equation. Other assumptions and the initial conditions are as above. The Buckley Leverett flow inside the porous medium as a function of time before breakthrough will be

$$V(t) = \phi S l_{ow}(t)[1 - \overline{S_w}(t)] \tag{22}$$

For the pressure drop over the core

$$\Delta P_{core} = \Delta P_{l_{ow}(t)} + \Delta P_{L-l_{ow}(t)} \tag{23}$$

To derive the first term (two-phase flow) of the pressure drop over the core two additional assumption are made: 1) no capillary forces and 2) no dip, so with

$$u_o = -\lambda_o \delta_x P \tag{24}$$

We get

$$u(t) f_o = -\lambda_o \delta_z P \tag{25}$$

Integrating over the length of the core subject to the two-phase flow

$$\Delta P_{l_{ow}(t)} = \frac{Q(t)\eta_o}{k_{ro}k} l_{ow}(t)\overline{f_o(S_w)} \tag{26}$$

Finally the total pressure drop becomes

$$\Delta P_{total} = \Delta P_c + \Delta P_{core} \tag{27}$$

The leak-off volume obeys the following equation:

$$Q_0 = [F_4 V(t) + 1]\frac{dV(t)}{dt} \tag{28}$$

This equation is similar to Equation 18 but in the present case the constant F_4 is given:

$$Q_0 = \frac{k}{\eta_w} S \frac{\Delta P}{L}; \qquad F_4 = \left[\frac{\eta_o \bar{f}_o(w)}{\eta_w k_{ro}(S_{wc})} - 1\right] \frac{1}{\phi\left(1 - \bar{S}_{w(t)}\right) SL} + \frac{\eta_o ck}{\eta_w k_c S\left(1 - c_p\right)(1 - \phi_c) L}$$

This function assumes that F_4 is constant which is a reasonable approximation. $\bar{S}_{w(t)}$ is the average water saturation as a function of time and $\bar{f}_o(w)$ is the average fractional flow of oil in the brine saturated core. Now the filtrate volume as a function of time is

$$V(t) = \begin{cases} Q_0 t & t < t_s \\ \dfrac{\sqrt{(F_4 V_s + 1)^2 + 2F_4 Q_0 (t - t_s)} - 1}{F_4} & t > t_s \end{cases} \tag{29}$$

When V_s and t_s equal zero, the equation for $t > t_s$ becomes:

$$V(t) = \frac{\sqrt{1 + 2F_4 Q_0 t} - 1}{F_4} \tag{30}$$

When $2F_4Q_0 >> 1$ equation 30 can be approximated as

$$V(t) = \sqrt{\frac{2Q_0 t}{F_4}} \tag{31}$$

Equation 31 shows the square root of time dependency of the filtrate volume after the spurt time.

Deep bed filtration

One idea behind the internal filtration is that not all the particles in the drilling fluid are able to pass through the pores of the core, because these particles are too large to pass through the narrow pore throats. A start for the deep bed filtration model is presented below. The size exclusion results in the external filter cake, the particles that are small enough filter into the porous medium. In equation form this becomes:

$$V = V_p^{fc} + V(t) + V_p^{pm} \tag{32}$$

In which V_p^{fc} is the volume of particles forming the external filter cake, V(t) the filtrated fluid volume and V_p^{pm} the volume of particles penetrating the porous medium. The volume of the external filter cake can also be written as

$$V_p^{fc} = c_1 V \tag{33}$$

$$V = \frac{V_p^{fc}}{c_1} = V_p^{fc} + V(t) + V_p^{pm} \tag{34}$$

$$V_p^{fc} = V_p^{fc} c_1 + c_1[V(t) + V_p^{pm}] \tag{35}$$

$$V_p^{fc} = \frac{c_1}{1 - c_1}[V(t) + V_p^{pm}] \tag{36}$$

Introducing the next equation for the external filter cake composition, with ϕ_c the filter cake porosity, S the cross-sectional area of filter cake and porous medium and l_c the length of the filter cake

$$V_p^{fc} = S(1 - \phi_c) l_c \tag{37}$$

Combining equation 40 and equation 41 gives the relation between the external filter cake and the fluid and particles filtering into the core

$$\frac{S l_c (1 - c_1)(1 - \phi_c)}{c_1} = V(t) + V_p^{pm} \tag{38}$$

The particles that do penetrate into the core follow the classic deep bed filtration model based on both the mass conservation equation and the kinetic equation (Herzig et al., 1970; Iwasaki, 1937; Sharma and Yortsos, 1987). To simply explain the model constant porosity, a negligible dispersion coefficient (D=0) and no particle diffusion are assumed. Studies have been conducted on the prediction of the filtration coefficient (Bedrikovetsky et al., 2004), but to present the model a constant filtration coefficient is used: $\lambda = \lambda_0$. The mass conservation law states

$$\phi \partial_t c + u \partial_z = (1 - \phi) \partial_t \sigma \tag{39}$$

And the kinetic equation to present the rate of deposition of particles

$$\partial_t \sigma = \lambda_0 u c \tag{40}$$

In the above equations ϕ is the porosity of the core, *t* is the time, *c* the concentration of suspended particles, *σ* the concentration of deposited particles, *z* the distance along the core and *u* the velocity. The solutions to the equations above are found with the following initial- and boundary conditions:

Initial conditions

$$c(z, t = 0) = 0 \; for \; z > 0$$

$$\sigma(z, t = 0) = 0 \; for \; z > 0$$

Boundary conditions

$$c(z = 0, t) = c_2 \; for \; t > 0$$

$$\sigma(z = 0, t) = 0 \; for \; t > 0$$

The solutions for *c(z,t)* and *σ(z,t)* are presented below, they are valid for *z<vt* and are both zero for *z>vt*, in which *v* is the interstitial velocity:

$$v = \frac{u}{\phi} \tag{41}$$

Solutions

$$c(z, t) = c_2 \exp(-Kz) \tag{42}$$

$$\sigma(z, t) = \phi \lambda_0 c_2 (vt - z) \exp(-Kz) \tag{43}$$

The total particle concentration inside the porous medium can be written as the sum of the suspended particles and deposited particles

$$C(z, t) = \phi c(z, t) + (1 - \phi)\sigma(z, t) \tag{44}$$

Appendix II: CT Scanner

To visualise the leak-off process in the core and to quantify the filtrate volume a CT scanner was used to scan the core at set times during the run of the experiments. The use of a CT scanner to visualise the filtration behaviour and fluid flow inside a porous medium has been proven before (Al-Abduwani et al., 2005; Saraf et al., 2010). The main concept of a CT scanner is sending out a beam of x-rays from different angles through the object of interest. The device measures the linear attenuation (μ [m^{-1}]) which describes the fraction of the x-rays that is scattered per unit thickness of the object of interest (Vinegar and Wellington, 1986) and creates a cross-sectional image of attenuation coefficients. The attenuation coefficient can be approximated by equation 45 and is the sum of Compton scattering and photoelectric contributions:

$$\mu = \rho \left[a + b \frac{Z^{3.8}}{E^{3.2}} \right] \tag{45}$$

In the above equation μ is the linear attenuation coefficient, ρ the electron density, *a* is the Klein-Nishina coefficient, *Z* the effective atom number, *E* the photon energy [keV] and *b* a constant.

In practise the attenuation is expressed in Hounsfield Units. A Hounsfield Unit (HU) is defined in equation 46, using the reference attenuation for water and air.

$$HU = 10^3 \left(\frac{\mu}{\mu_w} - 1 \right) \tag{46}$$

According to this equation the attenuation coefficients for water and air are H = 0 and H = 1000 respectively. The linear attenuation is dependent on the density of the material, making

$$\frac{\mu}{\rho} \tag{47}$$

the mass attenuation coefficient in $\left[\frac{cm^2}{g}\right]$. Dealing with mixtures and compounds this mass attenuation can be approximated by adding the values for the different elements according to their weight proportions (McCullough, 1975):

$$\frac{\mu}{\rho} = \sum_i w_i \left(\frac{\mu}{\rho} \right)_i \tag{48}$$

In which w_i is the fraction of weight of atom *i* in the mixture or compound.

Besides visualising the leak-off process and quantifying the filtration volume, the CT scan attenuation can be used to recover the porosity of the cores and the water saturation in the cores. The attenuation coefficient for a core filled with brine and oil will be:

$$\mu = (1 - \phi)\mu_s + \phi[S_w\mu_w + S_o\mu_o] \quad (49)$$

With

$$S_w + S_o = 1 \quad (50)$$

Then the attenuation coefficient as a function of the water saturation becomes

$$\mu(S_w) = (1 - \phi)\mu_s + \phi[\mu_o + (\mu_w - \mu_o)S_w] \quad (51)$$

If we take $S_o = 0$ then

$$\mu_{wet} = (1 - \phi)\mu_s + \phi\mu_w \quad (52)$$

And for a dry core the equation becomes

$$\mu_{dry} = (1 - \phi)\mu_s + \phi\mu_g \cong (1 - \phi)\mu_s \quad (53)$$

The porosity can be found subtracting equations 52 and 53

$$\phi = \frac{\mu_{wet} - \mu_{dry}}{\mu_w - \mu_g} = \frac{HU_{wet} - HU_{dry}}{HU_w - HU_g} \quad (54)$$

If we take $S_w = 0$, equation 51 becomes

$$\mu_{oil} = (1 - \phi)\mu_s + \phi\mu_o \quad (55)$$

Combining the equation above with equation 54 gives for the water saturation in the core

$$S_w = \frac{\mu_{(Sw)} - \mu_{oil}}{\phi(\mu_w - \mu_o)} = \frac{HU_{(Sw)} - HU_{oil}}{HU_w - HU_o} \quad (56)$$

Appendix III: Experimental Results

The figures in this appendix illustrate the experimental results for the repeat experiments discussed in the main body of the report.

1B: repeat experiment dry core

Here an overview of the results of the repeat experiment with a dry core, discussed in section 5.1, is displayed. The trend of images in Figure III - 1 is similar to the one for experiment 1A. The attenuation profiles in Figure III - 2 clearly show the decrease in drilling fluid level, associated with fluid leak-off, and the build-up of the external filter cake.

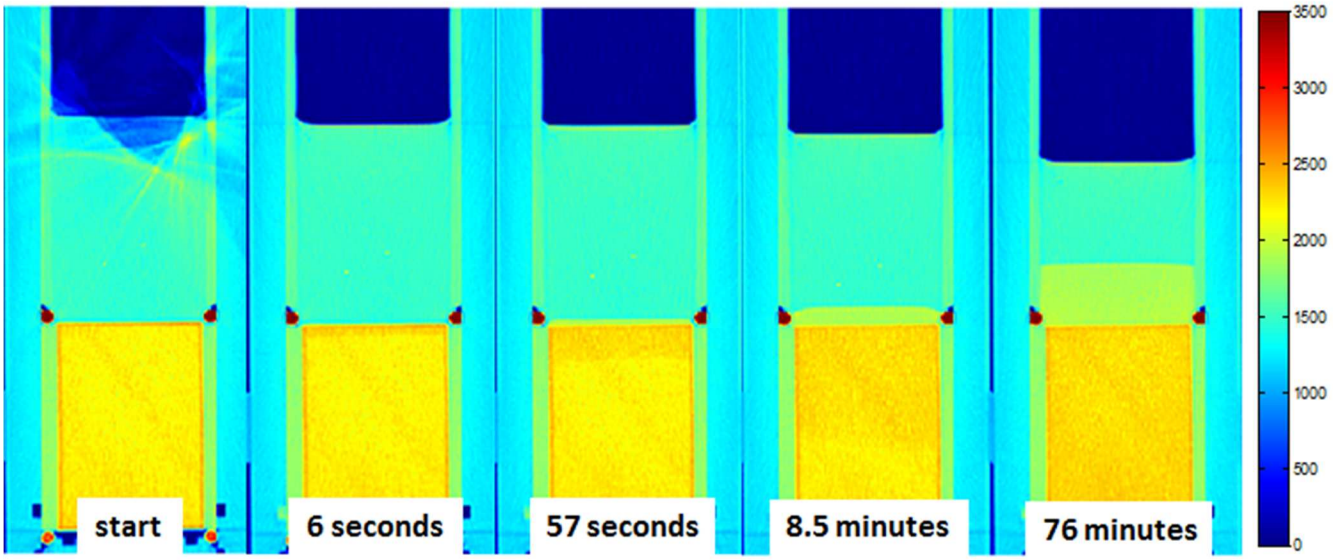

Figure III - 1: Five examples of CT scan images of experiment 1B at different times, visualising the leak-off process and used to construct the attenuation profiles

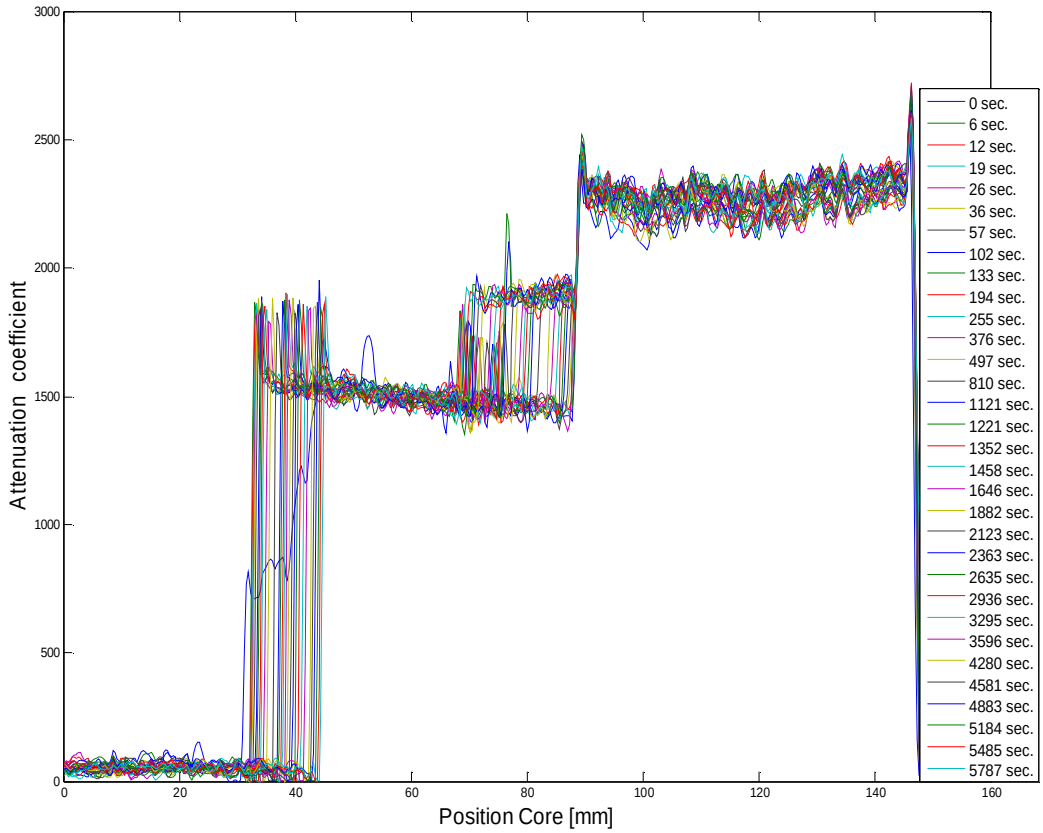

Figure III - 2: Attenuation profiles at different times for experiment 1B, created from CT scan images, used to determine the leak-off volume

1C: experiment with dril treat in drilling fluid

CT scans and attenuation profiles

To investigate the different behaviour between two wettability control agents, OmniChem and Dril Treat experiment 1C was done. Figure III - 3 shows CT scan images of experiment 1C, in total 16 images were shot in about 9 minutes. The start image demonstrates the shock wave as a result of pressurizing the system. On the top of the core immediately a small external filter cake can be distinguished and inside the core two interfaces are visible. The images of 6, 12 and 18 seconds show the leak-off process until the drilling fluid is finished. This behaviour is similar to the leak-off in the oil and fully brine saturated cores rather than the dry core. The last image shows the system after a bit more than two minutes, like in experiment 2A, the attenuation coefficient both of the external filter cake and inside the core differ from the other images. This can also be seen from Figure III - 4; in the middle and right part of the graph the wiggly curves belonging to later times jump to a lower attenuation coefficient, compared to earlier times. This can be explained by air entering the external filter cake and the core respectively; after all the drilling fluid is pushed through the both porous media by air, the air enters the external filter cake. The attenuation coefficient of air is lower than for drilling fluid, so the total attenuation coefficient becomes lower when air fills up the pores.

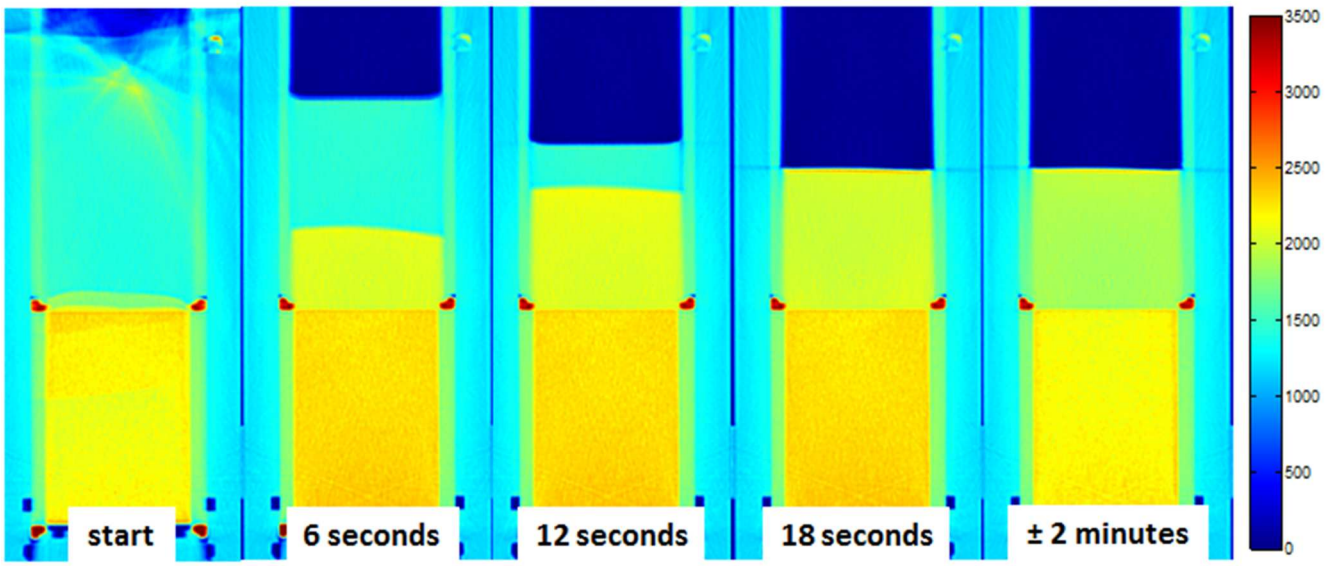

Figure III - 3: CT scan images of experiment 5 at different times, visualising the leak-off process and used to construct the attenuation profiles

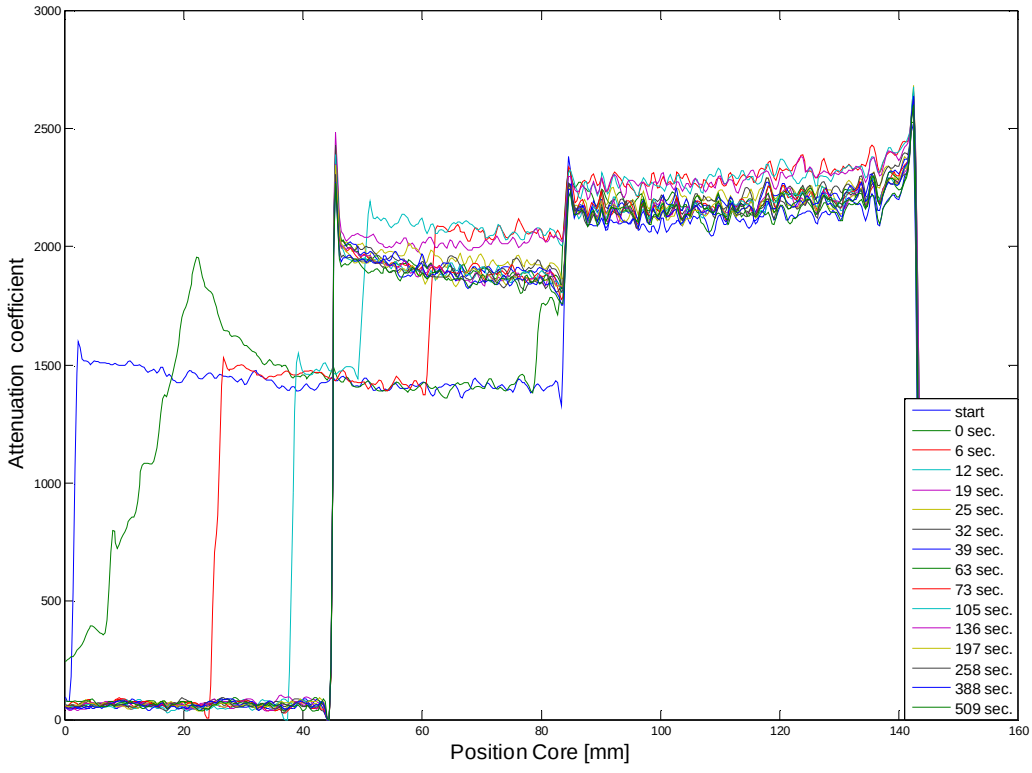

Figure III - 4: Attenuation profiles for experiment 5 at different times, created with CT scan images, used to determine the leak-off volume. The dark green curve (0 sec) is different from the other curves as this profile is influenced by the shock wave of pressurizing the system (see also the left most image in Figure III - 3)

External filter cake and internal filtration characterisation

The external filter cake thickness is 39 ± 0.5 mm (Figure III - 5). From the figure can be seen that the consistence of the external filter cake is very brittle. The top part of the external filter cake crumbled when it was removed from the corer holder. The crack visible at the bottom of the external filter cake is also a result of the removal procedure. The top part of the core and the bottom part of the external filter cake are used for the ESEM characterisation (Figure III - 6). From the top two images it can be seen that the external filter cake is not densely packed; the particles stick to each other without a clear orientation. The more enlarged picture shows a clear shape of the calcium carbonate particles and a low variety of particle sizes. The smaller particles do not seem to fill up the gaps between the larger particles; this can be dedicated to the absence of compaction. The larger image of the internal filtration shows similarity with the external filter cake, it can be concluded that a large part of the calcium carbonate also penetrates the core. This is backed up by the zoomed image of the internal filtration, which displays calcium carbonate attached to the grain. The external filter cake and internal filtration images show similarity with the ESEM images for experiment 3 (Figure 22).

Figure III - 5: Core and external filter cake (39 ± 0.5 mm) of experiment 1C; the filter cake is very brittle. By removing the core and external filter cake from the core holder the top of the external filter cake crumbled. At the bottom a crack is visible; this is caused by the removal from the core holder. The black ring is one of the O-rings used to seal the set-up.

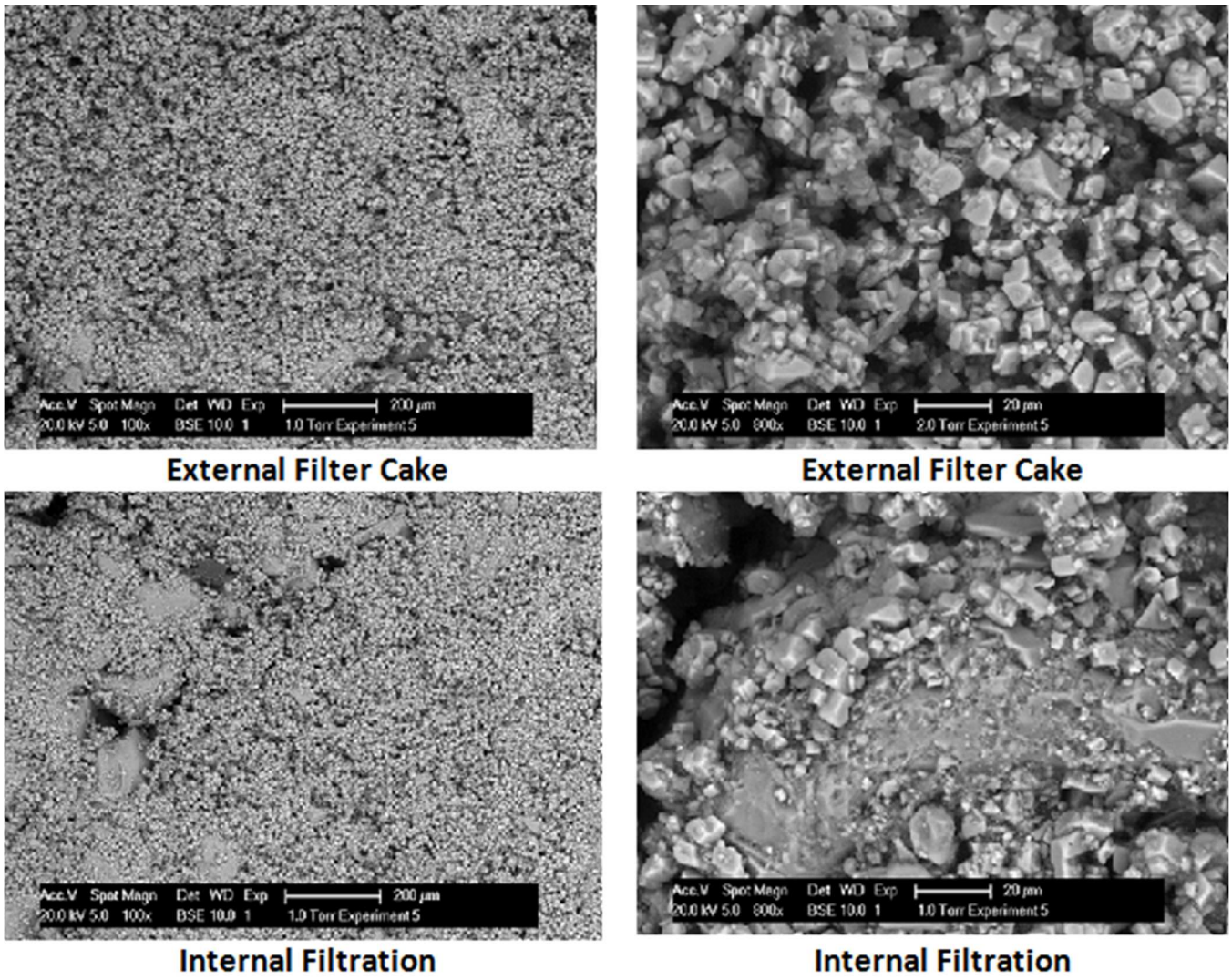

Figure III - 6: Images of external filter cake and internal filtration for experiment 1C, obtained by ESEM

Figure III - 7 shows the elemental analysis for the external filter cake and the internal filtration for experiment 5, in which the characteristic elements for the drilling fluid particles are displayed in weight percentage. This analysis confirms the large presence of calcium carbonate inside the core. Besides the calcium carbonate, bentonite and lime also penetrate the porous medium. It is clear the external filter cake contains the major part of the calcium carbonate. The marker elements for the particles used in the drilling fluid are displayed in Table 6.

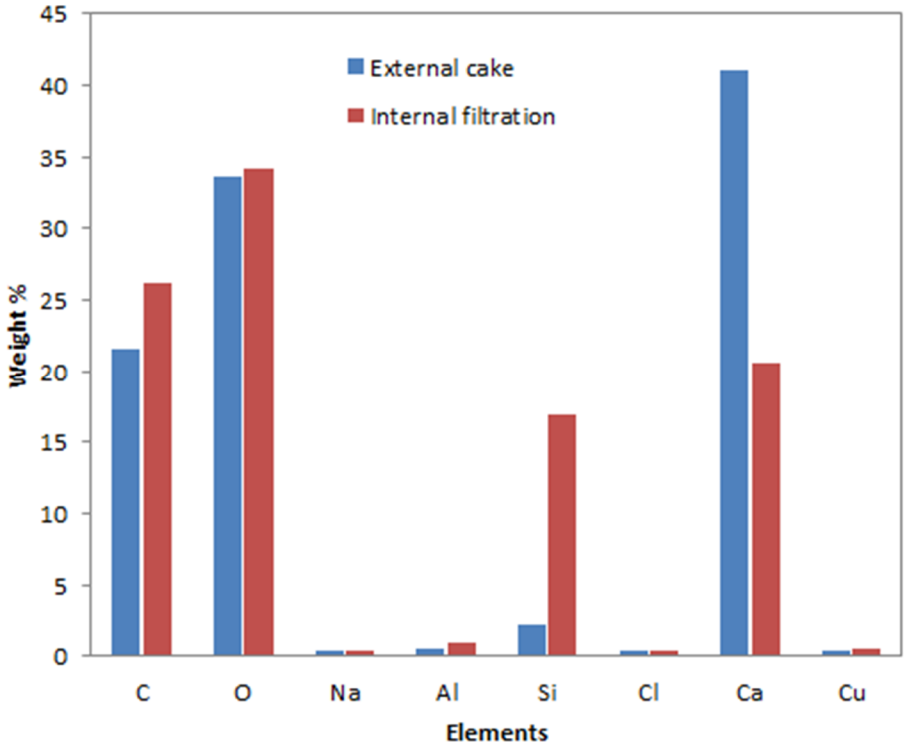

Figure III - 7: Elemental analysis for external cake and internal filtration of experiment 5, obtained by EDAX. The elements are displayed in weight %

2B: repeat experiment oil saturated core

Figure III - 8 displays an overview of the results of experiment 2B, it shows the same course in the images as for experiment 2A. A difference is the start volume of drilling fluid and therefore the experiment run time is less for experiment 2B, as is the height of the external filter cake in comparison with the results found in experiment 2A. In Figure III - 9 the attenuation profiles show the changing air-drilling fluid interface and the build-up of the external filter cake.

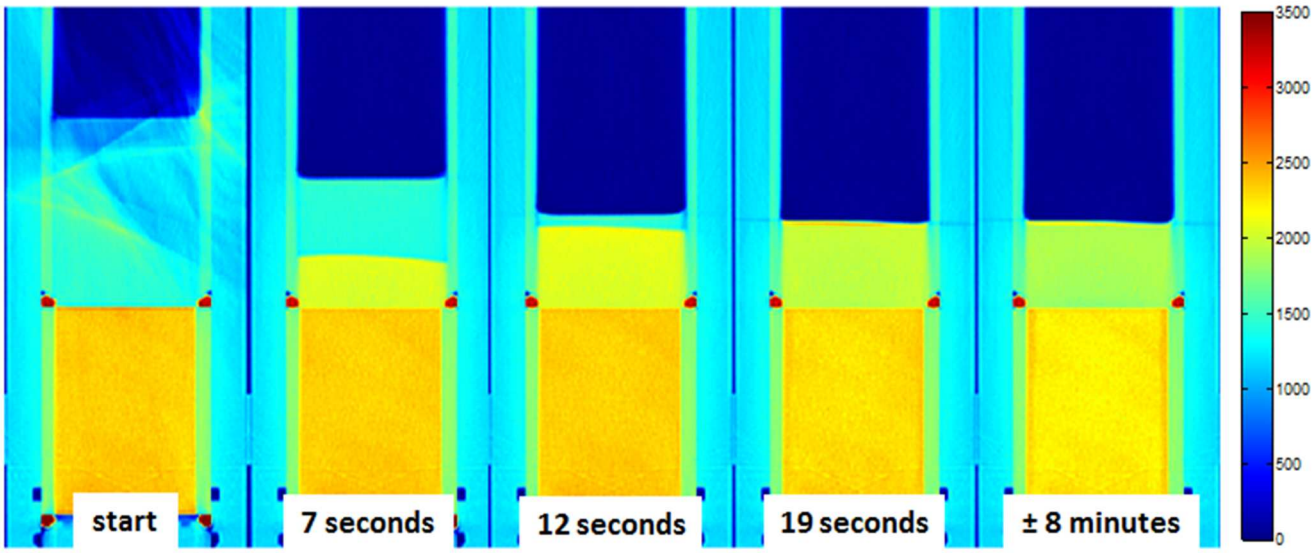

Figure III - 8: CT scan images of experiment 2B at different times, visualising the leak-off process and used to construct the attenuation profiles

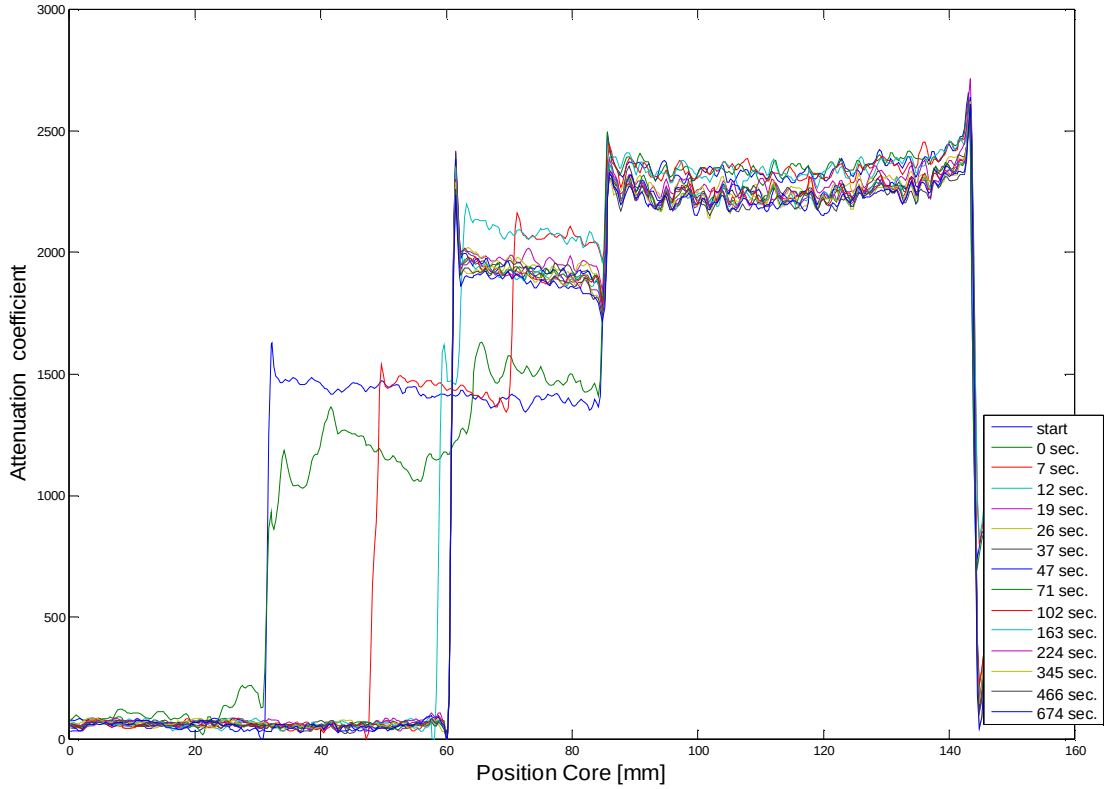

Figure III - 9: Attenuation profiles at different times for experiment 2B, created from CT scan images, used to determine the leak-off volume

3B: repeat experiment brine saturated core

Here an overview of the results of the repeat experiment with a brine saturated core, discussed in section 5.3, is displayed. The course of the images in Figure III - 10 are similar to the one for experiment 3A. A difference is the start volume of drilling fluid added to the core holder, this is less than start volume used in experiment 3A. The attenuation profiles in Figure III - 11 show the changing position of the air-drilling fluid interface as well as the external filter cake build-up.

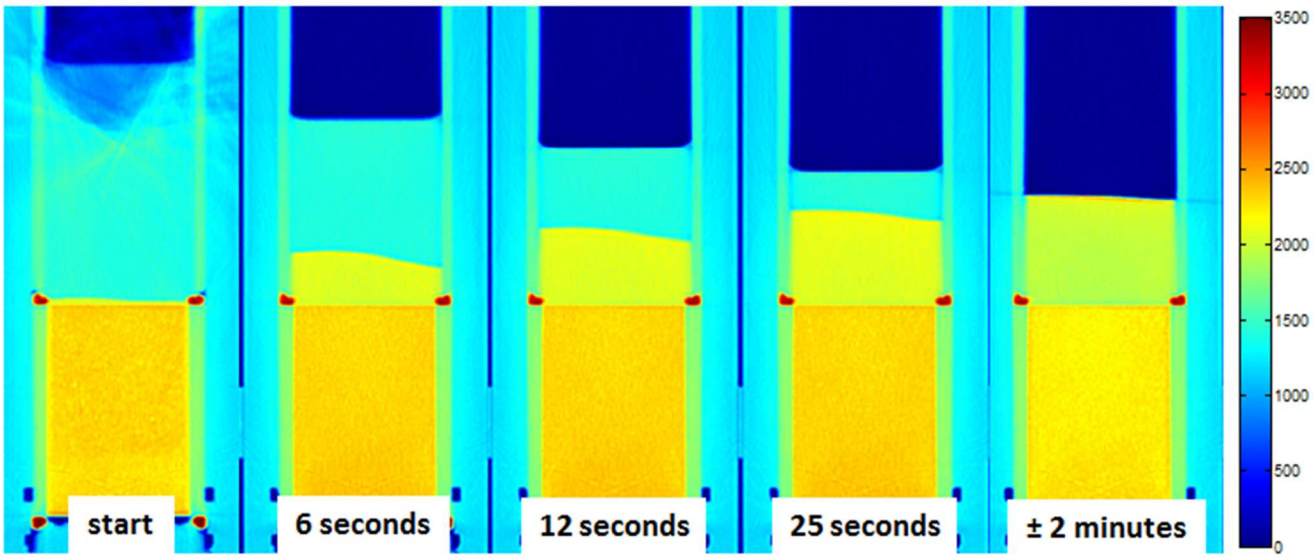

Figure III - 10: CT scan images of experiment 3B at different times, visualising the leak-off process and used to construct the attenuation profiles

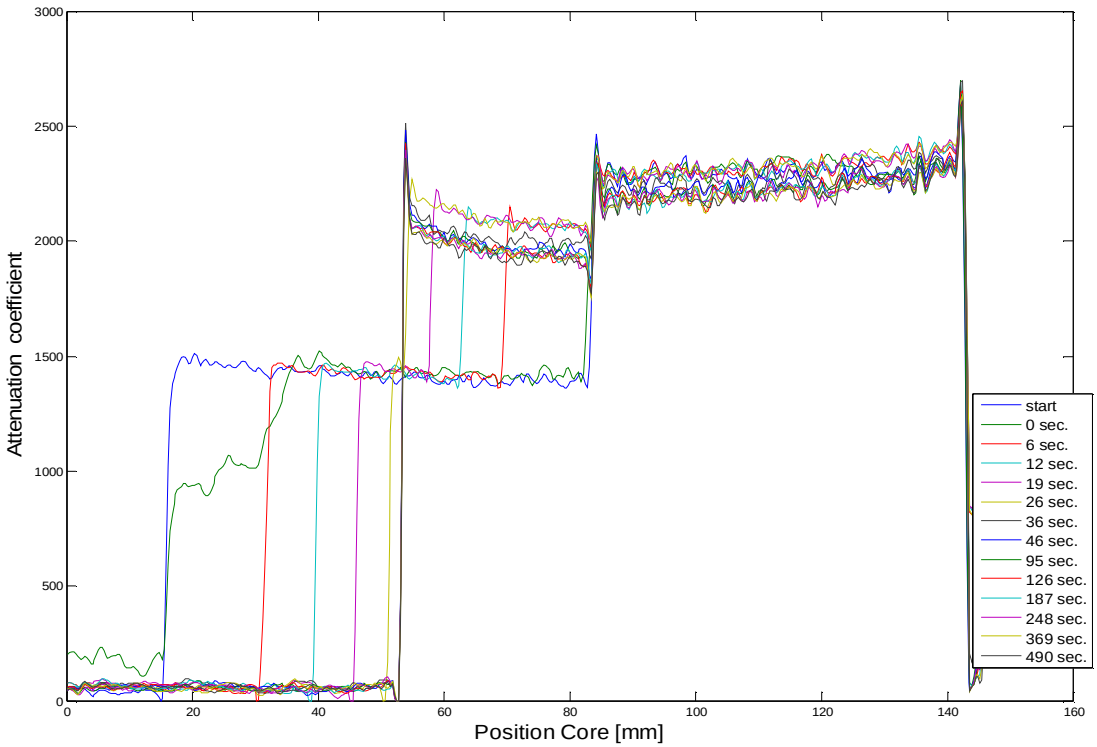

Figure III - 11: Attenuation profiles at different times for experiment 3B, created from CT scan images, used to determine the leak-off volume

4: Leak-off of Barite Drilling Fluid into a Brine Saturated Core

To verify that the results from experiments 2 and 3 are caused by addition of calcium carbonate and not due to the saturation of the cores experiment 4 (Table 5) is executed. For this experiment the additive in the drilling fluid is changed to barite, preserving the same volume percentage. An overview of the results is presented below, in total 23 images were shot in 41 minutes.

CT scan images and attenuation profiles

Figure III - 12 shows the CT scan images obtained during experiment 4. Very high attenuation coefficient of barite caused translucency artefacts and made it impossible to distinguish the external filter cake on the CT scan images. However it was possible to determine the leak-off volume from the movement of the air-drilling fluid interface (Figure III - 12). The attenuation profiles are of no use suffering from too much artefacts.

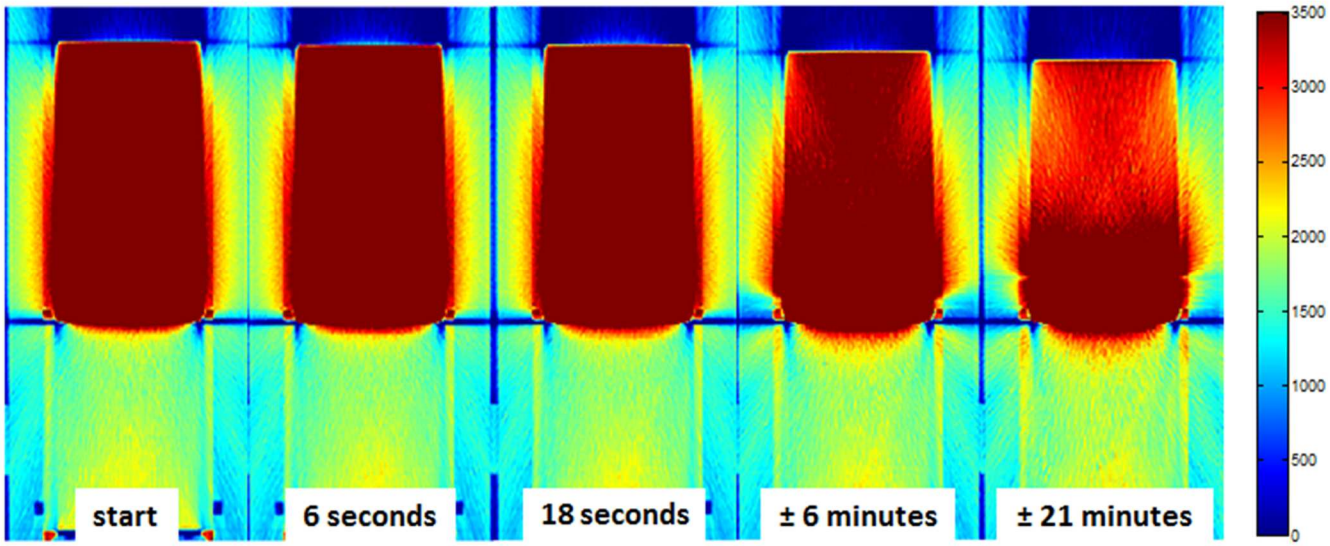

Figure III - 12: CT scan images of experiment 4 at different times, visualising the leak-off process and used to construct the attenuation profiles. No external filter cake can be distinguished due to the overwhelming attenuation response of barite

Leak-off volume

Figure III - 13 shows the filtration volume of experiment 4 as a function of the square root of time. By extrapolating the least squares linear fit the found spurt loss volume is 0.40 ± 0.05 ml. Although this is less than the spurt loss volume found in dry core experiments with barite as drilling fluid additive (see section 5.1), the main difference is the large continuing leak-off. After 26 minutes the leak-off volume counts 7.05 ± 0.05 ml, compared to 1.18 ± 0.05 ml and 1.52 ± 0.05 ml found in the dry core experiments performed by (van Overveldt 2011). This high leak-off rate shows similarity with experiment 3 but not to the same extent. In experiment 4 the leak-off volume has a steep slope as a function of the square root of time, but the fluid is not finished in a few minutes. As the leak-off volume after 41 minutes is only 8.64 ± 0.05 ml the effluent volume is also expected to be lower than seen in experiment 3. For experiment 4 an effluent volume of 2.8 ± 0.05 ml was found.

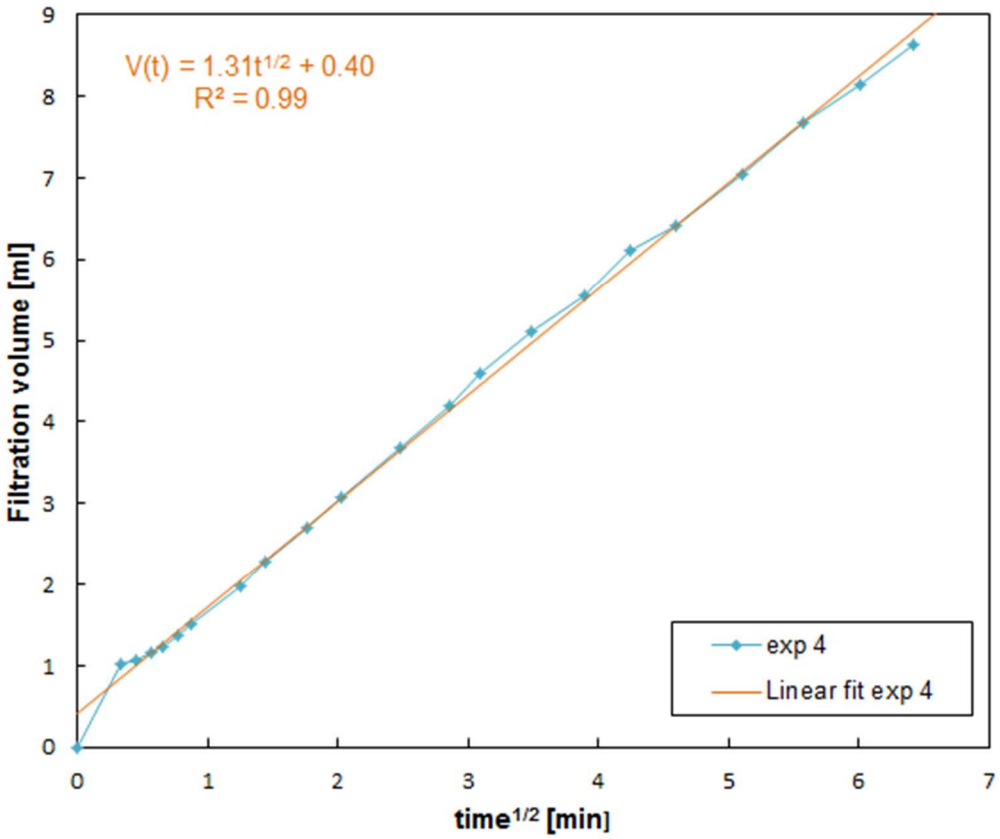

Figure III - 13: Filtration volume [ml] vs. the square root of time [min] for experiment 4, the spurt loss volume is 0.40 ± 0.05 ml

Figure III - 14: Top part of the core of experiment 4 and external filter cake (1.92 ± 0.05 mm)

External filter cake and internal filtration characterisation

The external filter cake thickness of 1.92 ± 0.05 mm (Figure III - 14) was found with ESEM. Figure III - 15 shows a part of that external filter cake, which consists of a variety of particle sizes and shapes. From the largest magnification it is seen that the particles build up a dense pack in which small particles fill in the gaps between larger particles. This can explain the low spurt loss volume and the low leak-off rate compared to the porous calcium carbonate filter cake.

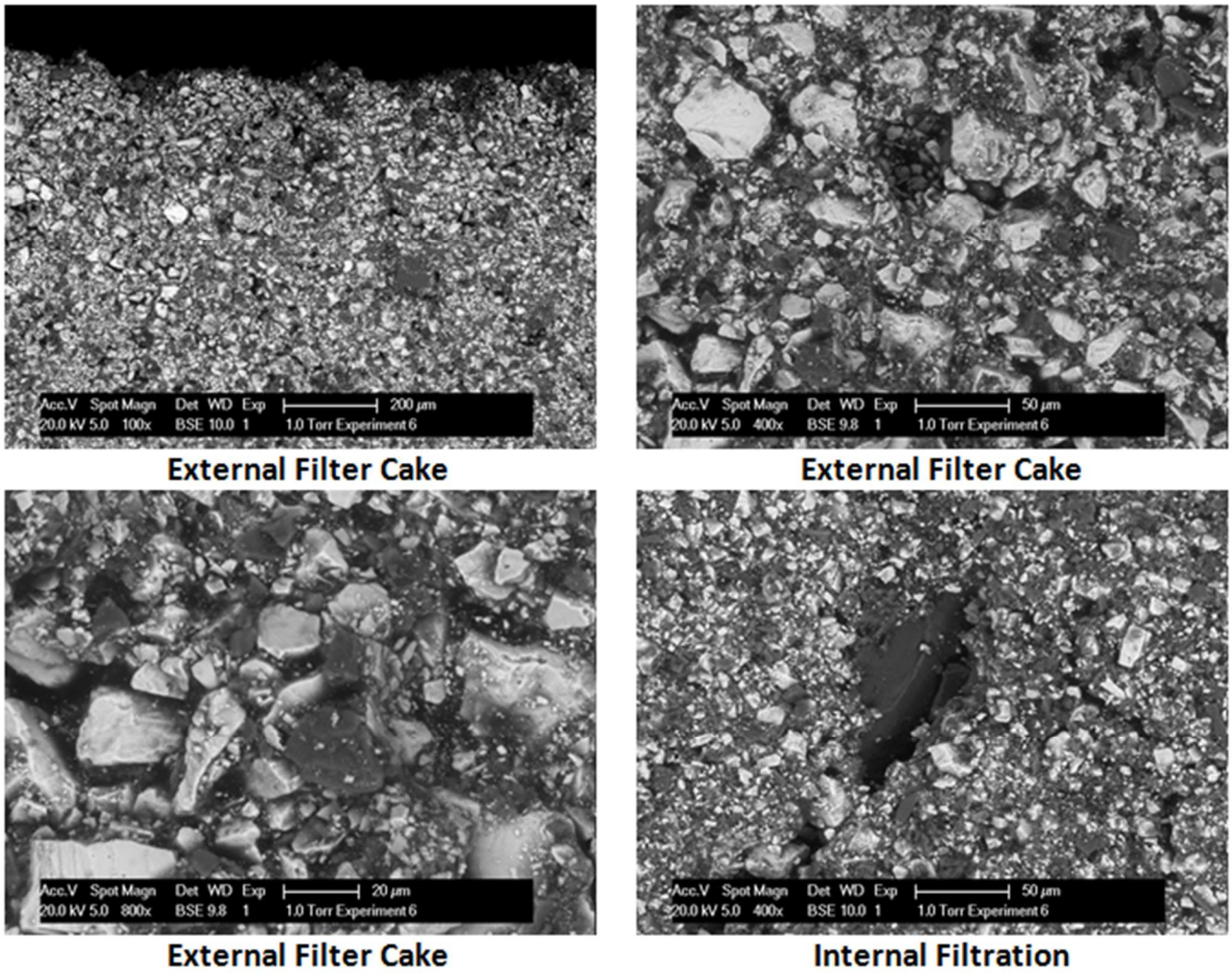

Figure III - 15: ESEM images of external filter cake and internal filtration for experiment 4

5B: repeat experiment brine saturated core with hematite in drilling fluid

An overview of the results of experiment 5B is displayed in Figure III - 16, showing a similar progress in the leak-off as seen in the images for experiment 5A (section 5.4). Here also a variation in attenuation colour can be distinguished at the top of the drilling fluid. Figure III - 17 shows the corresponding attenuation profiles, clearly indicating the spurt loss, the fluid leak-off and the external filter cake build-up.

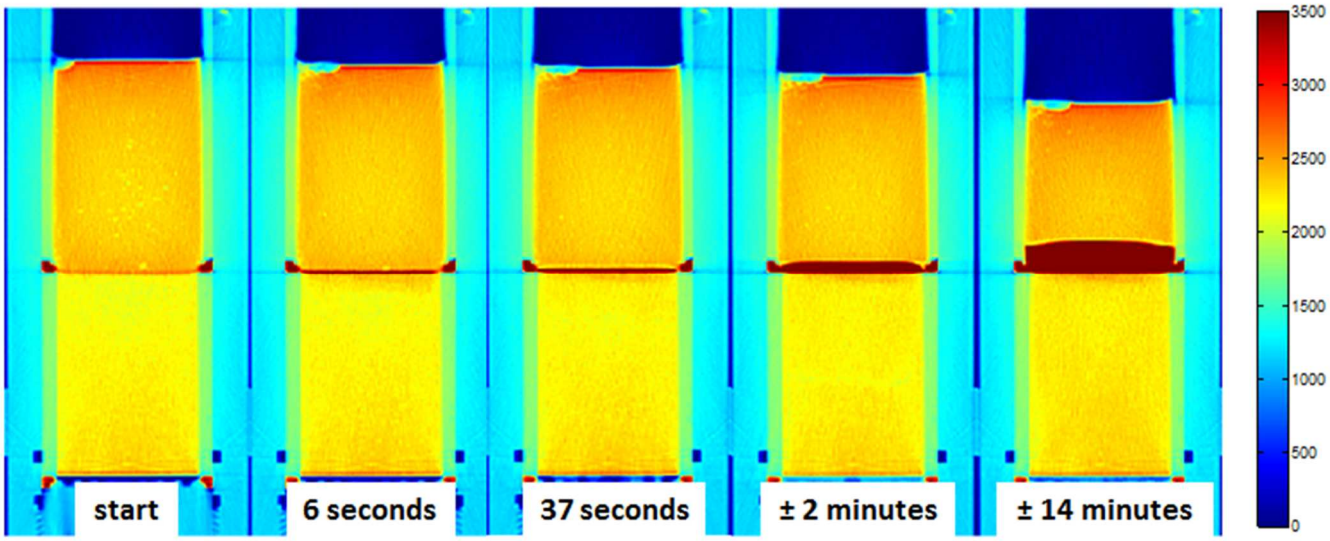

Figure III - 16: CT scan images of experiment 5B at different times, visualising the leak-off process and used to construct the attenuation profiles

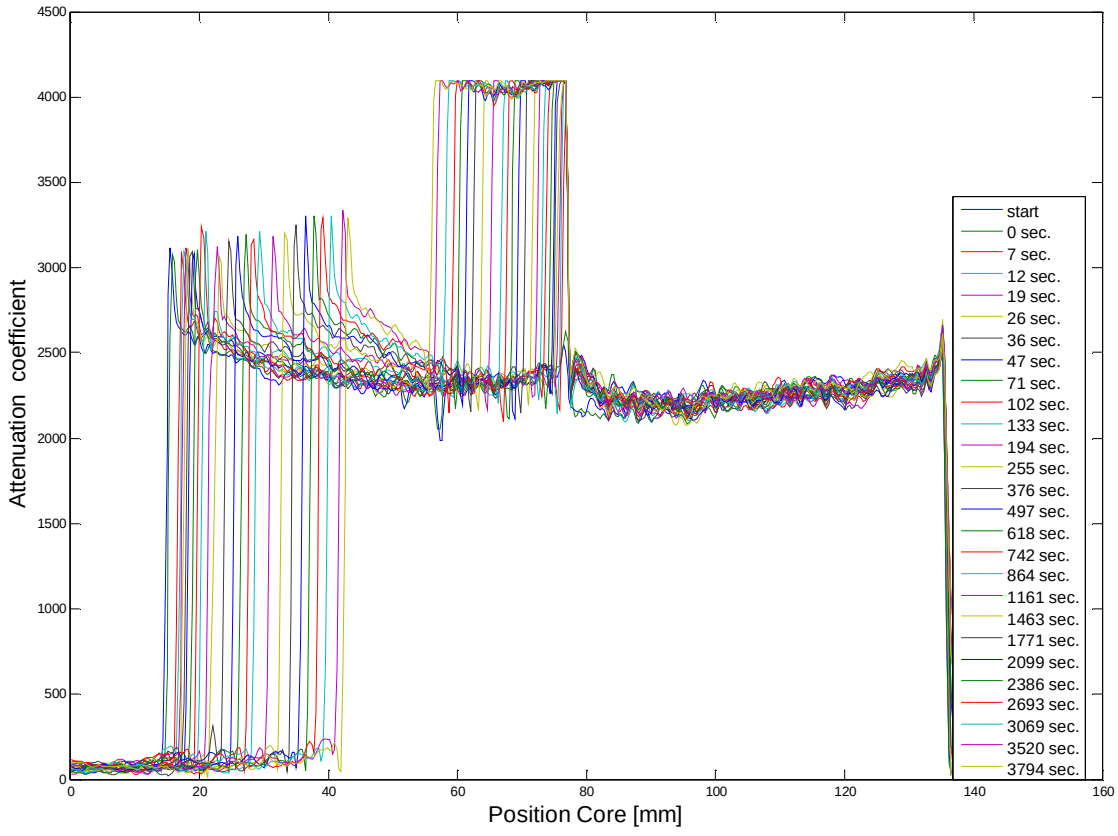

Figure III - 17: Attenuation profiles at different times for experiment 5B, created from CT scan images, used to determine the leak-off volume